1

Full title: **The EARP Complex and its Interactor EIPR-1 are Required for**

Cargo Sorting to Dense-Core Vesicles

Short title: **The EARP Complex Controls Dense-Core-Vesicle Biogenesis**

Irini Topalidou[1], Jérôme Cattin-Ortolá[1], Andrea L. Pappas[2], Kirsten Cooper[1],

Gennifer E. Merrihew[3], Michael J. MacCoss[3], Michael Ailion[1, *]

[1]Department of Biochemistry, University of Washington, Seattle, WA, USA

[2]Department of Neurobiology, Duke University School of Medicine, Durham, NC, USA

[3]Department of Genome Sciences, University of Washington, Seattle, WA, USA

[*]Correspondence: mailion@uw.edu

17   **Abstract**

18

19   The dense-core vesicle is a secretory organelle that mediates the regulated release of

20   peptide hormones, growth factors, and biogenic amines. Dense-core vesicles originate from the

21   trans-Golgi of neurons and neuroendocrine cells, but it is unclear how this specialized organelle is

22   formed and acquires its specific cargos. To identify proteins that act in dense-core vesicle

23   biogenesis, we performed a forward genetic screen in *Caenorhabditis elegans* for mutants

24   defective in dense-core vesicle function. We previously reported the identification of two

25   conserved proteins that interact with the small GTPase RAB-2 to control normal dense-core

26   vesicle cargo-sorting. Here we identify several additional conserved factors important for dense-

27   core vesicle cargo sorting: the WD40 domain protein EIPR-1 and the endosome-associated

28   recycling protein (EARP) complex. By assaying behavior and the trafficking of dense-core vesicle

29   cargos, we show that mutants that lack EIPR-1 or EARP have defects in dense-core vesicle

30   cargo-sorting similar to those of mutants in the RAB-2 pathway. Genetic epistasis data indicate

31   that RAB-2, EIPR-1 and EARP function in a common pathway. In addition, using a proteomic

32   approach in rat insulinoma cells, we show that EIPR-1 physically interacts with the EARP

33   complex. Our data suggest that EIPR-1 is a new component of the EARP complex and that

34   dense-core vesicle cargo sorting depends on the EARP-dependent retrieval of cargo from an

35   endosomal sorting compartment.

36

37 **Author Summary**

38   Animal cells package and store many important signaling molecules in specialized

39 compartments called dense-core vesicles. Molecules stored in dense-core vesicles include

40 peptide hormones like insulin and small molecule neurotransmitters like dopamine. Defects in the

41 release of these compounds can lead to a wide range of metabolic and mental disorders in

42 humans, including diabetes, depression, and drug addiction. However, it is not well understood

43 how dense-core vesicles are formed in cells and package the appropriate molecules. Here we use

44 a genetic screen in the microscopic worm *C. elegans* to identify proteins that are important for

45 early steps in the generation of dense-core vesicles, such as packaging the correct molecular

46 cargos in the vesicles. We identify several factors that are conserved between worms and humans

47 and point to a new role for a protein complex that had previously been shown to be important for

48 controlling trafficking in other cellular compartments. The identification of this complex suggests

49 new cellular trafficking events that may be important for the generation of dense-core vesicles.

50

Introduction

The dense-core vesicle is a specialized secretory organelle found in neurons and endocrine cells. In endocrine cells, these vesicles are often called secretory granules; for simplicity, we will here use the term 'dense-core vesicles' to refer to both the neuronal and endocrine carriers. Dense-core vesicles package several classes of cargo, including peptide hormones, growth factors, and biogenic amines. In response to elevated calcium, dense-core vesicles release their cargos to modulate a variety of biological processes ranging from blood glucose homeostasis to development, function and plasticity of the nervous system. Despite the importance of the signaling molecules released by dense-core vesicles, surprisingly little is known about how dense-core vesicles are generated and acquire their proper cargos (1–4).

Dense-core vesicles originate at the trans-Golgi network, but it is unclear how their compartmental identity is established and how cargos are correctly sorted into nascent dense-core vesicles. After budding from the trans-Golgi, immature dense-core vesicles undergo a poorly defined maturation process that involves homotypic vesicle fusion, peptide processing, and the removal of some soluble and transmembrane cargos (5–11). Some studies suggest that luminal dense-core vesicle cargos sort purely through an intrinsic ability to aggregate in the low pH/high Ca^{2+} milieu of the trans-Golgi (12), while other studies suggest that aggregation is not sufficient and that sorting relies on poorly defined structural motifs in cargo proteins that may interact with multiple sorting receptors (13,14). Two general models of dense-core vesicle cargo sorting have been debated for more than twenty years: the 'sorting by entry' and 'sorting by retention' models that propose that sorting occurs in the trans-Golgi as dense-core vesicles bud off, or in a post-Golgi step where non-dense-core vesicle cargos are removed (15,16). Experimental evidence supports both models, which are not mutually exclusive, suggesting that both mechanisms contribute to dense-core vesicle biogenesis.

4

76   Molecular mechanisms of dense-core vesicle biogenesis are poorly understood largely

77   because few proteins have been identified that function in this process. In recent years, the small

78   GTPase Rab2 has emerged as a major regulator of dense-core vesicle cargo trafficking. RAB-2,

79   its effector ICA69/RIC-19, and the putative RAB-2 GTPase-activating protein (GAP) TBC-8 have

80   all been shown to be important for early steps in dense-core vesicle cargo sorting at or near the

81   trans-Golgi (17–22). To identify additional factors in this pathway, we used a forward genetic

82   screen in the nematode *C. elegans* to isolate mutants that affect dense-core vesicle function. We

83   identified RUND-1, a RUN domain protein, and CCCP-1, a coiled-coil protein, that act as RAB-2

84   effectors to mediate normal dense-core vesicle cargo sorting (23). In mutants of *rab-2*, *rund-1*, or

85   *cccp-1*, morphologically normal dense-core vesicles are generated and transported to their axonal

86   release sites, but these dense-core vesicles have reduced levels of both luminal and

87   transmembrane cargos. RAB-2 and its effectors colocalize at or near the trans-Golgi, suggesting

88   that they act in the neuron cell body to mediate proper cargo-sorting as dense-core vesicles bud

89   off from the trans-Golgi or undergo post-Golgi maturation.

90   Here we investigate the function of several additional molecules identified in our genetic

91   screen for dense-core vesicle mutants: the conserved WD40 domain protein EIPR-1 and the VPS-

92   52 and VPS-53 subunits shared by the Golgi-associated retrograde protein (GARP) and

93   endosome-associated recycling protein (EARP) complexes. We show that EIPR-1 physically and

94   genetically interacts with the EARP complex. Mutants that lack EIPR-1 or EARP have defects in

95   dense-core vesicle cargo-sorting similar to those of mutants that lack RAB-2, RUND-1 or CCCP-1,

96   and genetic epistasis data indicate that they function in the same pathway. The requirement of

97   EARP for proper sorting of cargos to dense-core vesicles suggests that dense-core vesicle cargo

98   sorting is achieved in part through the retrieval of dense-core vesicle cargos or cargo receptors

99   from an endosomal sorting compartment. While there is ample prior evidence that cargos are

100   removed during dense-core vesicle maturation and trafficked to endosomes, our experiments

101   suggest that there is also trafficking back from endosomes to maturing dense-core vesicles.

102   **Results**

103

104   ***eipr-1* encodes a conserved WD40 domain protein**

105   To identify proteins required for dense-core vesicle biogenesis, we performed a forward

106   genetic screen in the nematode *C. elegans* based on suppression of the hyperactive locomotion of

107   an activated Gq mutant (23). We previously characterized the function of two novel conserved

108   proteins identified from this screen, RUND-1 and CCCP-1. Both RUND-1 and CCCP-1 interact

109   with the small GTP-binding protein RAB-2 when it is in its activated GTP-bound state (23).

110   Mutants in *rab-2*, *rund-1* and *cccp-1* have a stereotypical defect in locomotion behavior

111   characterized by little spontaneous movement on food, but coordinated slow locomotion when

112   stimulated. One additional uncloned mutant from our screen (*ox316*) had defects in locomotion

113   and egg-laying very similar to *rab-2*, *rund-1*, and *cccp-1* mutants. We cloned this mutant by single

114   nucleotide polymorphism (SNP) mapping and transgenic rescue experiments (Materials and

115   Methods). We named the gene *eipr-1* (EARP-interacting-protein, see below). The *eipr-1* mutant

116   phenotype is fully rescued by microinjection of the single gene Y87G2A.11, and the *ox316*

117   mutation leads to a premature stop codon in this gene (Figure 1A-C). We subsequently obtained a

118   deletion allele (*tm4790*) that causes identical locomotion and egg-laying phenotypes (Figure 1C;

119   Figure S1A). *eipr-1* encodes a novel WD40 domain protein of 362 amino acids (Figure 1B). Like

120   RUND-1 and CCCP-1, EIPR-1 has a single conserved ortholog in other metazoans. However,

121   unlike RUND-1 and CCCP-1, EIPR-1 is also found outside metazoans in plants and some fungi

122   and protozoa (Figure S2). Interestingly, EIPR-1 is not present in all protozoa and fungi, suggesting

123   an ancestral origin and loss in specific lineages including the budding yeast *Saccahromyces*

124   *cerevisiae*. The mouse *Eipr1* cDNA could also rescue the worm *eipr-1* mutant (Figure 1C; Figures

125   S1A), demonstrating functional conservation of the mammalian ortholog.

126

6

127 **EIPR-1 acts in the RAB-2 pathway to control locomotion and dense-core vesicle cargo**

128 **trafficking**

129 　　　The phenotypic similarities between *eipr-1* and *rab-2*, *rund-1*, and *cccp-1* mutants suggests

130 that these genes act in a common pathway. To test this, we built double mutants between *eipr-1*

131 and either *rab-2* or *rund-1* and assayed locomotion and egg-laying behavior. In both cases, the

132 double mutants do not show enhanced locomotion or egg-laying defects compared to the single

133 mutants (Figure 1D; Figure S1B). Thus, *eipr-1* acts in the *rab-2* pathway to control locomotion and

134 egg-laying behaviors.

135 　　　Mutants in *rab-2*, *rund-1* and *cccp-1* have reduced axonal levels of dense-core vesicle

136 cargos (19,22,23). To test whether *eipr-1* also acts in dense-core vesicle cargo trafficking, we

137 examined trafficking of both luminal and membrane cargos of dense-core vesicles. For luminal

138 cargos, we assayed the Venus-tagged peptides NLP-21, FLP-3, and INS-22. NLP-21 and FLP-3

139 are endogenous neuropeptides that undergo proteolytic processing (24,25), while INS-22 is an

140 insulin-family peptide that does not undergo proteolytic processing (26). For a membrane cargo,

141 we assayed GFP tagged IDA-1, the worm ortholog of the dense-core vesicle transmembrane

142 protein phogrin (27). Like the *rab-2* pathway mutants, we found that *eipr-1* mutants also had

143 reduced axonal levels of all luminal cargos and the transmembrane cargo IDA-1::GFP (Figure 2A-

144 D; Figure S3A-C). Double mutants of *eipr-1* with either *rab-2* or *rund-1* did not show an enhanced

145 defect compared to the single mutants (Figure 2A), again suggesting that *eipr-1* acts in the *rab-2*

146 pathway. To determine whether the *eipr-1* defect is specific to dense-core vesicle cargos, we

147 examined trafficking of the synaptic vesicle cargo UNC-17, the vesicular acetylcholine transporter.

148 *eipr-1* mutants showed no reduction in axonal levels of UNC-17 (Figure 2E). *eipr-1* mutants also

149 showed no reduction in axonal levels of the synaptic vesicle SNARE protein synaptobrevin (SNB-

150 1) (Figure S3D). We conclude that EIPR-1 acts in the RAB-2 pathway to specifically mediate

151 trafficking of dense-core vesicle cargos.

7

152 A mutation in the *egl-3* proprotein convertase blocks neuropeptide processing and leads to

153 an increase in axonal levels of luminal dense-core vesicle cargos (19,22). As with *rab-2* and *rund-*

154 *1*, there is increased axonal fluorescence of Venus-tagged NLP-21 in *eipr-1; egl-3* double mutants

155 as compared to the *eipr-1* single mutant (Figure 2F). However, the *egl-3* mutant on its own has

156 increased axonal fluorescence compared to wild-type, and the *eipr-1* mutant decreases axonal

157 fluorescence about 50% in either wild-type or *egl-3* backgrounds (Figure 2F), indicating that *eipr-*

158 *1*, like *rab-2* and *rund-1*, acts in parallel to *egl-3*. Thus, *eipr-1* mutants have reduced trafficking of

159 both processed and unprocessed cargos.

160

161 **EIPR-1 acts in neurons to control locomotion and dense-core vesicle biogenesis**

162 The behavioral and dense-core vesicle phenotypes of *eipr-1* mutants suggest that it acts in

163 neurons. Given that *eipr-1* is the fourth gene in an operon, it has been difficult to determine the

164 endogenous expression pattern of *eipr-1* (see Materials and Methods for details and Figure S4A).

165 Thus, we instead expressed the *eipr-1* cDNA under the control of neuronal-specific promoters to

166 determine whether the gene functions in neurons. Expression of *eipr-1(+)* under the neuronal

167 specific *rab-3* promoter fully rescued *eipr-1* mutant locomotion, dense-core vesicle trafficking, and

168 egg-laying (Figure 3A,B and data not shown). Expression of *eipr-1(+)* under the cholinergic *unc-17*

169 promoter also rescued the locomotion defect. Expression in cholinergic motor neurons (using the

170 *acr-2* promoter) did not rescue the locomotion phenotype, but expression driven by a head-

171 specific derivative of the *unc-17* promoter (*unc-17Hp*) rescued the locomotion phenotype,

172 indicating that *eipr-1* acts mainly in head cholinergic neurons to regulate locomotion behavior

173 (Figure 3A). The dense-core vesicle trafficking defect of *eipr-1* mutants is cell autonomous, as

174 expression of *eipr-1(+)* driven by the *unc-129* promoter fully rescued the axonal trafficking defect

175 of NLP-21::Venus expressed by the same *unc-129* promoter (Figure 3B). Thus, EIPR-1 acts in

176 neurons to control dense-core vesicle trafficking at the cellular level and locomotion behavior at

177 the organismal level.

178   The cell-specific constructs described above had EIPR-1 C-terminally tagged with GFP.

179   Because these constructs were able to rescue the mutant phenotype, the EIPR-1::GFP protein

180   must be functional; thus we examined these strains to determine the subcellular localization of

181   EIPR-1. Unlike RAB-2, RUND-1 and CCCP-1 which are localized predominantly to the trans-Golgi

182   (19,22,23), EIPR-1::GFP was expressed diffusely throughout the cytoplasm when expressed

183   under such promoters as *rab-3* or *unc-17*, even when coexpressed with a GTP-locked mutant of

184   RAB-2 (Figure S4B,C). However, given that endogenously tagged EIPR-1 is undetectable (see

185   Materials and Methods), these EIPR-1::GFP constructs are almost certainly overexpressed even

186   though they are single-copy insertions, and the lack of localization could be an artifact of this

187   overexpression. Thus, although the genetic interactions indicate that EIPR-1 acts in the RAB-2

188   pathway, it is unclear whether EIPR-1 colocalizes with RAB-2 and its interactors.

189

190   **EIPR-1 interacts with members of the GARP and EARP trafficking complexes**

191   WD40 domain proteins typically act as scaffolds that mediate multiple protein-protein

192   interactions (28). Given the genetic interactions seen between *eipr-1* and members of the *rab-2*

193   pathway, we asked whether the EIPR-1 protein shows physical interactions with any of the RAB-2

194   pathway proteins. Using yeast two-hybrid assays, we did not detect interactions between EIPR-1

195   and RAB-2, RUND-1 or CCCP-1. RAB-2 and RUND-1 were also localized normally in *eipr-1*

196   mutants (data not shown). Thus, neither cellular localization nor physical interactions connect

197   EIPR-1 directly to RAB-2 or its interactors, suggesting that EIPR-1 may act at a distinct step in this

198   trafficking pathway.

199   To identify interactors of EIPR-1, we expressed GFP-tagged rat EIPR1 in the rat insulinoma

200   cell line 832/13 and performed mass spectrometry on GFP pulldowns. 832/13 cells package

201   insulin into dense-core secretory granules that closely resemble neuronal dense-core vesicles and

202   share similar mechanisms of biogenesis, maturation, and release (29,30). Mammalian orthologs of

9

203   RAB-2, RUND-1, CCCP-1 and EIPR-1 are all expressed endogenously in 832/13 cells (Figure

204   4A), so these cells are a reasonable place to look for interactors of these proteins.

205   We performed two independent pulldowns of GFP-tagged rat EIPR1. The top four hits

206   identify the proteins VPS51, VPS50 (also known as syndetin or VPS54L), VPS52, and VPS53

207   (Figure 4B; Figure S5). Also high on the list is VPS54. These five proteins define the related

208   GARP and EARP trafficking complexes that share the VPS51, VPS52, and VPS53 proteins, but

209   use either VPS54 or VPS50 as a fourth subunit (31–33). Thus, EIPR1 is likely tied closely to one

210   or both of these complexes, neither of which has been previously linked to dense-core vesicle

211   biogenesis. These proteomic results are especially striking because, as described below, we had

212   independently identified the *vps-52* and *vps-53* genes in our forward genetic screen for dense-

213   core vesicle mutants.

214   To confirm the interactions detected by mass spectrometry, we performed

215   coimmunoprecipitation experiments. GFP-tagged EIPR1 expressed in 832/13 cells

216   coimmunoprecipitated with either mCherry-tagged VPS51 or with endogenous VPS50 (Figure

217   4C), validating the interactions. Since no other proteins showed as strong an interaction by mass

218   spectrometry as the GARP/EARP subunits, EIPR1 is a specific interactor of the GARP/EARP

219   complexes.

220

221   **The GARP/EARP subunits VPS-51, VPS-52 and VPS-53 act in the RAB-2 pathway to control**

222   **locomotion and dense-core vesicle cargo trafficking**

223   Further supporting the model that EIPR-1 functions with either the GARP or EARP

224   complex, we isolated mutants in the worm orthologs of *vps-52* and *vps-53* in our original forward

225   genetic screen. We cloned these mutants by mapping, whole-genome sequencing, and transgenic

226   rescue (see Materials and Methods). Both the *vps-52(ox345)* and *vps-53(ox339)* mutants are

227   predicted to be molecular nulls, an early stop and deletion respectively, and both mutants

228   phenocopy other deletion mutants in the same genes. These mutants also resemble a deletion

10

229   mutant in the *vps-51* gene. Neuronal roles of *vps-51*, *vps-52*, and *vps-53* have not been previously

230   described in *C. elegans*.

231   We tested whether *vps-51*, *vps-52* and *vps-53* mutants have behavioral and cellular

232   phenotypes similar to those of *eipr-1* and *rab-2*. Like *eipr-1* and members of the *rab-2* pathway,

233   *vps-51*, *vps-52* and *vps-53* mutants have slow but coordinated locomotion (Figure 5A) and an

234   egg-laying defect. A double mutant between *rab-2* and *vps-53* did not have a stronger locomotion

235   phenotype than the *rab-2* single mutant (Figure 5B), indicating that *rab-2* and *vps-53* act in the

236   same pathway to control locomotion. These mutants also exhibit defects in trafficking dense-core

237   vesicle cargos. Like *rab-2* and *eipr-1*, *vps-51*, *vps-52* and *vps-53* mutants all show reduced axonal

238   levels of Venus-tagged NLP-21 or FLP-3 peptides (Figure 5C,D; Figure S6). A *rab-2; vps-53*

239   double mutant did not show an enhanced NLP-21::Venus trafficking defect compared to the single

240   mutants (Figure 5E), also suggesting that *rab-2* and *vps-53* act in the same pathway. However,

241   unlike the *rab-2* and *eipr-1* mutants which show reduced axonal accumulation of the dense-core

242   vesicle transmembrane protein IDA-1, mutants in *vps-51*, *vps-52* and *vps-53* all show increased

243   axonal accumulation of IDA-1 (Figure 5F), indicating that these genes have at least some function

244   distinct from *rab-2* or *eipr-1*. Since VPS-51, VPS-52, and VPS-53 are common to both GARP and

245   EARP, these data suggest that GARP, EARP, or both are required for normal dense-core vesicle

246   biogenesis and regulation of worm locomotion.

247   To determine the expression pattern of *vps-52* and *vps-53*, we made transgenic worms

248   expressing the YFP-derivative Citrine under either the *vps-52* or *vps-53* promoter. Both *vps-52*

249   and *vps-53* were expressed strongly and widely in neurons and were also expressed in several

250   other tissues (Figure 6A,B and Materials and Methods for details). These data are consistent with

251   the reported expression patterns of *vps-51*, *vps-52*, and *vps-53* (34). To determine where VPS-52

252   and VPS-53 localize in neurons, we tagged them with tagRFP at their C-termini and expressed

253   them under their own promoters as single-copy transgenes to achieve endogenous expression

254   levels. Both VPS-52 and VPS-53 localized mainly to two or three perinuclear puncta in neuronal

11

255   cell bodies (Figure 6C,D), reminiscent of the localization of RAB-2, RUND-1 and CCCP-1 to the

256   trans-Golgi (23). We examined colocalization of VPS-52::tagRFP or VPS-53::tagRFP with GFP-

257   tagged RAB-2 and found that they are partially overlapping in worm neurons (Figure 6C,D),

258   consistent with the reported localization of GARP to the trans-Golgi in other cell types and other

259   systems (Conibear and Stevens, 2000; Liewen et al., 2005; Lobstein et al., 2004; Luo et al.,

260   2011).

261

262   **The EARP complex controls cargo sorting to dense-core vesicles**

263   To determine whether it is GARP or EARP (or both) that is required for dense-core vesicle

264   biogenesis, we obtained deletion mutations in the GARP-specific *vps-54* and EARP-specific *vps-*

265   *50* subunits. Unlike the other GARP mutants, *vps-54* mutants did not have defects in locomotion

266   or axonal accumulation of the luminal dense-core vesicle cargos NLP-21 and FLP-3 (Figure 7A,C;

267   Figure S7A,B). In contrast, *vps-50* mutants had defects in locomotion and reduced axonal levels

268   of luminal dense-core vesicle cargos very similar to those of mutants in *eipr-1*, *vps-51*, *vps-52* and

269   *vps-53* (Figure 7A-C; Figure S7B). An *eipr-1; vps-50* double mutant did not have an enhanced

270   defect in locomotion or dense-core vesicle cargo trafficking when compared to the *vps-50* single

271   mutant (Figure 7A,B; Figure S7B), indicating that *eipr-1* and *vps-50* act in the same pathway.

272   Moreover, like *eipr-1*, mutations in *vps-50* did not affect axonal levels of the synaptic vesicle

273   protein synaptobrevin (Figure S7C), indicating that VPS-50 is not required for the trafficking of

274   synaptic vesicle proteins. In 832/13 cells, endogenous VPS50 showed a perinuclear localization

275   that partially overlapped GFP-tagged RAB2A and CCCP1 (Figure S8A,B). Providing additional

276   evidence that *vps-50* acts in the dense-core vesicle pathway regulating worm locomotion, we

277   found that a *vps-50* mutation suppressed the activated Gq mutant *egl-30(tg26)* that was used in

278   the genetic screen for dense-core vesicle mutants. However, a *vps-54* mutation did not suppress

279   this activated Gq mutant. Taken together, these data support a role for EARP, but not GARP, in

280   dense-core vesicle biogenesis and regulation of worm locomotion.

12

281   The decreased axonal levels of luminal dense-core vesicle cargos like NLP-21::Venus

282   could be due either to decreased levels of the cargo in dense-core vesicles, or to increased

283   release of the cargo. Exocytosis of dense-core vesicles and release of their cargos is reflected by

284   accumulation of NLP-21::Venus in scavenger cells called coelomocytes that reside in the body

285   cavity of the worm (35,36). Thus, we measured coelomocyte fluorescence as an indirect measure

286   of dense-core vesicle release. Like *rab-2* mutants, *eipr-1, vps-50*, and *vps-52* mutants all showed

287   reductions in the accumulation of Venus fluorescence in coelomocytes that is approximately

288   proportional to the decrease in axonal fluorescence seen in these mutants (Figure S9). This

289   suggests that these mutants are not defective in dense-core vesicle release per se, but release

290   reduced amounts of dense-core vesicle cargo because the vesicles contain less cargo.

291   Additionally, double mutants between *eipr-1* and *rab-2* or *vps-50* did not have stronger

292   coelomocyte uptake phenotypes than the single mutants, providing further evidence that these

293   genes all act in the same dense-core vesicle cargo sorting pathway.

294   Two independent *vps-50* mutants exhibited either a slight decrease or no decrease in

295   axonal levels of the dense-core vesicle transmembrane cargo IDA-1 (Figure 7D). Thus, *vps-50*

296   and *eipr-1* have a similar IDA-1 trafficking phenotype that is distinct from the increased axonal

297   accumulation of IDA-1 seen in *vps-51, vps-52* and *vps-53* mutants. Interestingly, *vps-54* mutants

298   showed no change in axonal accumulation of IDA-1 (Figure 7D).

299   Previously, *C. elegans* GARP mutants, including *vps-54*, were shown to have enlarged

300   lysosomes in coelomocytes (34). We examined *eipr-1* and *vps-50* mutants for this phenotype

301   using the lysosomal marker LMP-1::GFP expressed in coelomocytes. Unlike GARP mutants,

302   neither *eipr-1* nor *vps-50* had enlarged lysosomes (Figure S10), indicating that EARP is not

303   required for normal lysosomal morphology. Thus, GARP is required for normal lysosomal

304   morphology and EARP is required for dense-core vesicle biogenesis.

305

306   **Discussion**

13

307   In this study, we identified several new factors important for dense-core vesicle biogenesis:

308   the WD40 protein EIPR-1 and the EARP trafficking complex with which it interacts. EIPR-1 and

309   EARP are required for normal trafficking of dense-core vesicle cargos, and act in the same

310   genetic pathway as the small GTP-binding protein RAB-2 and its interactors RUND-1 and CCCP-

311   1. Loss of any of these proteins results in reduced levels of cargo in mature dense-core vesicles

312   and associated behavioral defects. The identification of EARP, an endosomal recycling complex,

313   suggests that dense-core vesicle cargo trafficking involves not only the forward trafficking of cargo

314   into nascent dense-core vesicles as they bud off from the trans-Golgi, but also the retrieval or

315   recycling of cargo or sorting factors from endosomal compartments (Figure 8).

316

317   **The WD40 domain protein EIPR1 is a new interactor of the EARP complex**

318   Through a convergence of worm genetics and proteomics in rat 832/13 cells, we identified

319   the WD40 domain protein EIPR1 as a direct physical and functional interactor of the EARP

320   complex. The EARP complex was recently identified as a new complex structurally related to the

321   GARP complex (32,33). EARP shares the VPS51, VPS52 and VPS53 subunits with the GARP

322   complex, but uses VPS50 instead of VPS54 as a fourth subunit. VPS50 was also recently shown

323   to interact with GARP subunits in three large-scale mass spectrometry interactome data sets,

324   demonstrating that the EARP complex is present in various cell types in several species (37–39).

325   In two of these data sets, EIPR1 was shown to interact with EARP subunits in human HEK293T or

326   HeLa cells (37,38), providing support for our results and indicating that the EIPR1 interaction with

327   EARP is robust and conserved. In fact, using VPS50 as a bait protein, VPS51, VPS52, VPS53

328   and EIPR1 were pulled down as a stoichiometric complex (37), indicating that EIPR1 may form

329   part of a stable complex with EARP. No VPS54 was pulled down. This is consistent with our

330   genetic experiments showing that *eipr-1* and *vps-50* mutants have similar locomotion and dense-

331   core vesicle cargo trafficking phenotypes that are shared by *vps-51*, *vps-52*, and *vps-53* mutants,

332   but not *vps-54*. Thus, we propose that EIPR1 is a new member of the EARP complex.

14

333   The human *Eipr1* gene was originally named *Tssc1* for "tumor-suppressing subtransferable

334   candidate 1" because it was first identified as one of several genes thought to be candidates for a

335   tumor-suppressing activity on chromosome 11 (40). However, when the human genome was

336   completed, *Tssc1* was located on chromosome 2, and thus could not be the putative tumor

337   suppressor. Because the TSSC1 protein appears to be both physically and functionally connected

338   to the EARP complex, we propose that it be renamed EIPR1 (EARP-Interacting PRotein).

339   WD40 domain proteins typically act as scaffolds that provide several interaction surfaces

340   for the assembly of larger protein complexes (28). Though EIPR1 clearly interacts with EARP, it is

341   unclear whether EIPR-1 is required for the localization or stability of the EARP complex. In an

342   *eipr-1* mutant, VPS-52 still showed a punctate localization (Figure S11), though this could also

343   reflect its participation in the GARP complex. In *C. elegans* (unlike yeast), the remaining members

344   of the GARP complex were shown to be stable and localized in the absence of one of the subunits

345   (34), so the same may hold true for EARP. Surprisingly, GFP-tagged EIPR-1 was found

346   throughout the cytoplasm when overexpressed in *C. elegans* neurons and not associated with a

347   membrane-bound compartment. However, overexpression of membrane-localized proteins can

348   sometimes lead to a diffuse cytoplasmic appearance (41). Because we could not detect an

349   endogenously tagged EIPR-1::GFP fusion protein, we presume that *eipr-1* is normally expressed

350   at low levels. This conclusion is supported by the few cDNAs or RNAseq reads reported for *eipr-1*

351   on Wormbase (http://www.wormbase.org/species/c_elegans/gene/WBGene00013599#0df9-gec6-

352   2).

353   One other hit found in both of our EIPR1 pulldowns is SNAP29, a late Golgi/endosomal

354   SNARE protein that has been shown to function in endocytic recycling and autophagosome fusion

355   (42–45). SNAP29 was also identified as an interactor of EIPR1 or EARP subunits (but not VPS54)

356   in other recent mass spectrometry studies (33,37,38), and we confirmed that SNAP29 interacts

357   with EIPR1 by a coimmunoprecipitation experiment (Figure S12). GARP has been shown to

358   interact with several late-Golgi SNARE proteins and has been proposed to both tether vesicles

15

359   and promote SNARE assembly that leads to fusion (34,46–49). We propose that SNAP29 is part

360   of a SNARE complex specifically interacting with EARP.

361

362   **A new role for the GARP/EARP complex in mediating dense-core vesicle cargo sorting**

363   EARP was originally shown to be localized to a Rab4 positive endosomal compartment in

364   both fly S2 cells and rat hippocampal neurons (32,33), and depletion of the EARP-specific VPS50

365   subunit led to a modest defect in the endocytic recycling of the transferrin receptor back to the cell

366   surface (33). Here we identify a new neuronal role of this complex in the sorting of cargos to

367   dense-core vesicles.

368   The GARP complex was originally characterized as an endosome to Golgi retrograde

369   trafficking complex that may tether endosome-derived vesicles at the trans-Golgi (46,48,50,51).

370   Loss or depletion of GARP subunits leads to a variety of phenotypes that are presumed to be

371   secondary to a primary defect in retrograde trafficking, including missorting of lysosomal proteins,

372   abnormal lysosomal morphology, defective autophagy, defective lipid and sterol transport,

373   defective anterograde transport of glycosyl phosphatidylinositol (GPI)-anchored and

374   transmembrane proteins, and defects in sphingolipid homeostasis (31,34,47,50–53).

375   GARP and EARP subunits are expressed especially strongly in the nervous system in both

376   mice and worms (33,34,54,55), but until now, neuronal phenotypes of GARP/EARP mutants have

377   not been carefully characterized. However, several mutations in GARP/EARP subunits have been

378   connected to neurological diseases. Mutations in VPS54 and VPS52 lead to neurological

379   disorders in mice that have been studied as models of the human diseases amyotrophic lateral

380   sclerosis (ALS) and the seizure disorder high-pressure nervous syndrome, respectively (56,57).

381   Also, mutations in the human VPS53 gene cause progressive cerebello-cerebral atrophy type 2

382   (PCCA2), a neurodegenerative disease characterized by severe mental retardation and early-

383   onset epilepsy (58). It will be interesting to determine whether the GARP/EARP mutations cause

384   these diseases due to their previously characterized role in sorting lysosomal cargos (50,51), or

385   due to their newly identified role in dense-core vesicle biogenesis. It will also be interesting to

386   determine whether neurological diseases associated with VPS52 and VPS53 are caused by

387   dysfunction of GARP or EARP or both. The overt behavioral phenotypes of *C. elegans* mutants

388   affecting the GARP/EARP common subunits (*vps-51*, *vps-52* and *vps-53*) are very similar to those

389   of *vps-50* and *eipr-1*, suggesting that EARP is more important than GARP for neuronal function in

390   *C. elegans*.

391   Our identification of EIPR-1 and EARP as important for dense-core vesicle cargo sorting

392   supports a recent study that showed that *vps-50* mutants have locomotion and dense-core vesicle

393   cargo trafficking defects (55). Like *eipr-1*, the slow locomotion of *vps-50* mutants on food was

394   partially rescued by expression in cholinergic neurons (55), suggesting that *eipr-1* and *vps-50*

395   function together in the same neurons to control locomotion behavior. VPS-50 was also shown to

396   physically interact with the vacuolar-ATPase (v-ATPase) complex that acidifies dense-core

397   vesicles, and *vps-50* mutants had defects in vesicle acidification and assembly of the v-ATPase

398   complex (55). These defects may be indirectly caused by a primary defect of EARP mutants in

399   missorting dense-core vesicle cargos, possibly including subunits of the v-ATPase.

400   How does EARP sort dense-core vesicle cargos? Thus far, all of the factors in the RAB-

401   2/EARP pathway are cytoplasmic proteins that localize to membranes but do not have

402   transmembrane domains and thus cannot communicate directly with luminal cargos inside the

403   vesicles. Thus, either there is a transmembrane sorting receptor yet to be identified or the RAB-

404   2/EARP pathway proteins help sort cargo by a passive mechanism that does not involve direct

405   interactions with cargo. We favor a model based on the latter idea (Figure 8). This model

406   combines and builds on aspects of the well-described 'sorting by entry' and 'sorting by retention'

407   models for cargo sorting to dense-core vesicles (15,16). Specifically, we propose that cargo

408   sorting occurs through the following steps: (1) an intrinsic ability of certain dense-core vesicle

409   cargos to aggregate in the trans-Golgi (sorting by entry), (2) additional aggregation in immature

410   dense-core vesicles as the luminal pH is reduced and propeptides are processed into their mature

411 forms, and (3) the repeated recycling of non-aggregated cargo from immature dense-core vesicles

412 through an endosomal compartment back to the trans-Golgi/immature dense-core vesicles. Such

413 a recycling pathway will help sort away soluble non-dense-core vesicle cargos (sorting by

414 retention), and also help concentrate aggregated dense-core vesicle cargos by providing these

415 cargos multiple chances to aggregate and be retained by mature dense-core vesicles. We

416 propose that EARP and the RAB-2 pathway may control the trafficking into or out of the

417 endosomal compartment. In mutants in this pathway, increased trafficking of cargos to

418 endosomes or reduced retrieval of cargos from endosomes leads to their ultimate loss to

419 lysosomes and hence reduced cargo levels in mature dense-core vesicles. Thus, EARP and the

420 RAB-2 pathway do not act instructively to sort cargos in the way a sorting receptor would, but

421 instead have a permissive role, somewhat analogous to the mechanism by which chaperones

422 assist protein folding by providing proteins multiple chances to fold correctly and avoid

423 degradation. Such a permissive role for EARP and the RAB-2 pathway would be consistent with

424 the fact that none of these mutants has a complete loss of cargo sorted to the mature dense-core

425 vesicles that accumulate in axons.

426   Several previous studies provide support for our model. Following dense-core vesicle

427 exocytosis, the dense-core vesicle transmembrane protein peptidylglycine α-amidating

428 monooxygenase (PAM) has been shown to be recycled back to dense-core vesicles via

429 endosomal compartments (59), demonstrating that there must be trafficking of cargos from

430 endosomes to dense-core vesicles. Our model builds on this observation to suggest that such

431 endosomal trafficking occurs not only following exocytosis, but also during the biogenesis of

432 dense-core vesicles. Another study demonstrated that soluble dense-core vesicle cargos are

433 segregated from self-aggregating cargos in immature dense-core vesicles near the trans-Golgi

434 (60), consistent with the idea that aggregation of cargos at this point in vesicle maturation can be

435 sufficient to drive sorting into mature dense-core vesicles.

436

18

A growing number of proteins important for dense-core vesicle biogenesis

The identification of EIPR-1 and EARP adds to a growing list of proteins that have been recently identified as being involved in mediating aspects of dense-core vesicle biogenesis. In *C. elegans*, we and others previously identified the small GTPase RAB-2; the putative RAB-2 GAP TBC-8; the RAB-2 effectors RIC-19, RUND-1 and CCCP-1; and the membrane-associated Golgi-localized protein HID-1 (19,20,22,23,61,62). Mutations in all of these proteins result in similar defects in dense-core vesicle cargo trafficking, and genetic epistasis data support the idea that they function in a common pathway.

In other systems, a number of factors have been recently identified as having roles in dense-core vesicle biogenesis. These include factors that belong to protein families implicated in various aspects of membrane trafficking such as BAR domain proteins (18,21,63,64), members of the Arf family of small GTPases (65), the clathrin adaptor complexes AP-1 and AP-3 (66–69), members of the BLOC-1 and HOPS complexes that are important for the biogenesis of lysosome-related organelles (70–72), and members of the sortilin family of lysosomal sorting receptors (73,74). Among these, there are a few possible connections to the RAB-2/EARP pathway we have described in *C. elegans*. AP-1 is involved in trafficking between various cellular compartments, most notably between the trans-Golgi and endosomes (75), and has been shown to be associated with immature dense-core vesicles (6,8), so it may be involved in the endosomal recycling pathway proposed by our model. The BLOC-1 subunit dysbindin was identified as an interactor of EIPR1, VPS51 and VPS53 by mass spectrometry (38), and the possible dense-core vesicle coat protein VPS41 (along with other HOPS subunits) was identified as an interactor of Rab2 (32).

One final factor shown to be important for dense-core vesicle biogenesis in mouse chromaffin cells is the SNARE protein Vti1a (76). Interestingly, Vti1a is one of the components of a trans-Golgi SNARE complex that binds GARP (48), and it also localizes to immature dense-core vesicles near the trans-Golgi (76). Syntaxin 6, another member of this SNARE complex, has also been shown to be associated with immature dense-core vesicles and small vesicles near the

19

463   trans-Golgi or endosomes (8,11,77). Blocking antibodies to syntaxin 6 were shown to inhibit the

464   homotypic fusion of immature dense-core vesicles in an *in vitro* fusion assay (11), but the

465   physiological importance of syntaxin 6 for dense-core vesicle biogenesis *in vivo* remains unclear.

466   Interestingly, the RAB-2 effector RUND-1 is tightly colocalized with syntaxin 6 in *C. elegans*

467   neurons (23) and the BAR domain protein PICK1 tightly colocalized with syntaxin 6 in mouse

468   pituitary cells (21). Also, syntaxin 6 physically interacts with SNAP29 (11), a SNARE protein that

469   we and others identified as an EIPR1 or EARP interactor (33,37,38). It will be interesting to

470   determine whether SNAP29, Vti1a, and syntaxin 6 are members of a SNARE complex that

471   interacts with EARP, and the compartment where they function.

472

473   **Materials and methods**

474

475   **Strains**

476   Worm strains were cultured and maintained using standard methods (Brenner, 1974). A

477   complete list of strains and mutations used is provided in the Strain List (Table S1).

478

479   **Isolation and identification of *eipr-1*, *vps-52*, and *vps-53* mutations**

480   The *eipr-1(ox316)*, *vps-52(ox345)* and *vps-53(ox339)* mutants were isolated in an ENU

481   screen for suppressors of the hyperactive locomotion of an activated Gq mutant, *egl-30(tg26)* (23).

482   When outcrossed away from the *egl-30(tg26)* mutation, all three of these mutants had sluggish

483   unmotivated locomotion and defects in egg-laying. The phenotypes of all three of these mutants

484   are partially maternally rescued; for example, the phenotype of an *eipr-1* mutant is weaker if its

485   parent is heterozygous (*eipr-1/+*) than if its parent is homozygous (*eipr-1/eipr-1*). The basis of this

486   maternal rescue is not clear, but indicates the likely maternal deposition of these proteins in the

487   egg.

488   We mapped these mutations using single nucleotide polymorphisms (SNPs) in the

489   Hawaiian strain CB4856 as described (Davis et al., 2005). The *eipr-1(ox316)* mutation was

490   mapped to a 205 kb region on the right arm of chromosome I with 31 predicted protein-coding

491   genes. Because there was no coverage of this region by *C. elegans* cosmids, we obtained *C.*

492   *briggsae* BACs (from CHORI) carrying orthologs of the genes in this region and injected them into

493   *eipr-1(ox316)* mutants. The BAC RPCI94_01L06 rescued the *eipr-1* locomotion defect, while the

494   BAC RPCI94_13K10 did not. RPCI94_01L06 carries orthologs of six *C. elegans* genes in the

495   mapped region. We sequenced the best two candidate genes in the *ox316* mutant and found a C

496   to T transition mutation in exon 4 of Y87G2A.11, leading to a premature stop codon at Q310. We

497   obtained and sequenced the *eipr-1* cDNA from the ORFeome library, confirming the gene

498   structure predicted on Wormbase. The clone carried a single mutation that we fixed by Quick

21

499 Change mutagenesis. We then cloned the mutation-free cDNA into a Gateway entry vector for use

500 in rescue experiments. We rescued the *ox316* mutant with a transgene carrying only Y87G2A.11,

501 confirming the gene identification.

502 The *vps-52(ox345)* mutation was mapped to a 720 kb region in the middle of the X

503 chromosome with 122 genes. The *vps-53(ox339)* mutation was mapped to a 92 kb region in the

504 middle of chromosome III with 23 genes. We constructed a double mutant strain carrying both the

505 *ox339* and *ox345* mutations and performed Illumina whole-genome sequencing. Within the region

506 where *ox339* mapped, we found no SNPs predicted to alter protein function, but did identify a 687

507 bp deletion within the T05G5.8 (*vps-53*) ORF. Within the region where *ox345* mapped, we found

508 only a single SNP predicted to alter protein function, a C to T transition mutation in the F08C6.3

509 (*vps-52*) ORF that created a premature stop codon at S119. The mutations in the *vps-53* and *vps-*

510 *52* genes were confirmed by Sanger sequencing. We confirmed the gene identifications by

511 performing complementation tests with other deletion mutations in each gene and by performing

512 single-gene rescue experiments.

513

514 **Molecular biology and transgenes**

515 A complete list of constructs is provided in the Plasmid List (Table S2). Most of the

516 constructs were made using the three slot multisite Gateway system (Invitrogen). Typically, a

517 promoter, a coding sequence (genomic DNA or cDNA), and an N- or C-terminal fluorescent tag

518 (GFP or tagRFP-T) were cloned along with a 3'UTR into the pCFJ150 destination vector used for

519 Mos1-mediated single copy insertion (MosSCI) on chromosome II at *ttTi5605* (78,79). All

520 insertions were made by the direct injection MosSCI method. For most constructs, we isolated

521 multiple independent insertions that behaved similarly. Extrachromosomal arrays were made by

522 standard transformation methods (80).

523

524 **Expression of *eipr-1*, *vps-52*, and *vps-53***

22

525   *eipr-1* is the fourth gene in an operon about 30 kb downstream from the start of the first

526   gene in the operon, so it is not clear what promoter regulates *eipr-1*. We made a construct driving

527   expression of GFP by the promoter region upstream of the first gene of the operon (1348 bp

528   upstream of the W09C5.1 start codon). Extrachromosomal arrays of this construct showed

529   expression in several tissues including the intestine, pharynx and hypodermis (Figure S4A), but

530   not neurons, suggesting that this promoter fusion does not represent the endogenous expression

531   pattern of *eipr-1*. We also tagged the chromosomal *eipr-1* gene with GFP using the CRISPR/Cas9

532   method (81). However, neither N-terminal nor C-terminal GFP-tagged *eipr-1* was bright enough to

533   detect, even with the use of an anti-GFP antibody to amplify the signal, indicating that *eipr-1* is

534   likely to be expressed endogenously at low levels.

535   We made constructs driving expression of the yellow-fluorescent protein Citrine under the

536   *vps-52* and *vps-53* promoters and generated worms with extrachromosomal arrays. For *vps-52,*

537   822 bp upstream of the start codon was used as a promoter. *vps-53* is the second gene in an

538   operon downstream of the gene *gcc-2*. For *vps-53*, 4502 bp upstream of the *gcc-2* start codon

539   was used as the promoter. *vps-52* showed strong expression in neurons in the head, ventral cord,

540   and tail (Figure 6A), as well as expression in the pharynx, intestine, uterus, spermatheca, skin,

541   and several muscle types (body wall, vulval). Other than the skin and muscle expression, this

542   expression pattern matches that of *rund-1* (23). *vps-53* was not as strongly expressed, but was

543   clearly visible in many head neurons (though possibly not all), ventral cord neurons, tail neurons,

544   the pharynx, and weakly in the body wall muscles (Figure 6B).

545

546   **Locomotion and egg-laying assays**

547   To measure locomotion, first-day adults were picked to thin lawns of OP50 bacteria,

548   allowed to rest for 30 seconds, and then body bends were counted for one minute. A body bend

549   was defined as the movement of the worm from maximum to minimum amplitude of the sine wave

550   (82).

23

551   To measure egg-laying, L4 larvae were placed on plates with OP50 and allowed to mature

552   at 25°C overnight. The next day, five adult animals were moved to a fresh plate and allowed to lay

553   eggs at 25°C for 2.5 hours. The number of eggs present on the plate was then counted.

554

555   **Cell culture**

556   The INS-1-derived 832/13 cell line (83) was obtained from Dr. Christopher Newgard (Duke

557   University School of Medicine) via Dr. Ian Sweet and Dr. Duk-Su Koh (University of Washington).

558   832/13 cells were routinely grown at 5% CO2 at 37°C in RPMI-1640, GlutaMAX^{TM} (GIBCO),

559   supplemented with 10% FBS, 1 mM Sodium pyruvate, 10 mM HEPES, 0.0005% 2-beta-

560   mercaptoethanol, and 1X Pen/Strep (GIBCO). Cells were passaged biweekly after trypsin-EDTA

561   detachment. All studies were performed on 832/13 passages between 70 and 90. 832/13 cells

562   were transfected using Lipofectamine 2000 (ThermoFisher) according to the manufacturer's

563   instructions.

564

565   **Expression and purification of anti-GFP nanobody**

566   The anti-GFP nanobody was expressed and purified as previously described (84) with few

567   modifications. In brief, bacterial expression vector pLaG16 containing the anti-GFP nanobody was

568   transformed in Arctic Express (DE3) cells (Agilent). Cells were induced with 0.1 mM IPTG for 16 h

569   at 8°C and centrifuged at 5,000g for 10-min at 4°C. To isolate the periplasmic fraction by osmotic

570   shock (85), cells were incubated for 1h in TES buffer (0.2 M Tris-HCl pH 8, 0.2 mM EDTA and 0.5

571   M sucrose). Cells were spun down for 10 min at 6,000g at 4°C and the pellet was suspended in

572   TE buffer (0.2 M Tris-HCl pH 8 and 0.5 mM EDTA) following a 45 min incubation. Cells were

573   pelleted by a 30 minutes spin at 30,000g at 4°C. The supernatant (periplasmic fraction) was

574   bound to PerfectPro Ni-NTA Agarose affinity resin (5 Prime) for 1h at 4°C. The resin was washed

575   once with wash buffer I (20 mM sodium phosphate pH 8.0, 0.9 M NaCl) and twice with wash buffer

576   II (20 mM sodium phosphate pH 8.0, 150 mM NaCl and 10 mM imidazole) and eluted with His

577   elution buffer (20 mM sodium phosphate pH 8.0, 150 mM NaCl, 250 mM imidazole). The eluent

578   was then dialyzed with PBS. Recombinant anti-GFP nanobody was conjugated to epoxy-activated

579   magnetic Dynabeads M270 (Life Technologies) using 10 µg recombinant protein per 1 mg of

580   Dynabeads, with conjugations carried out in 0.1 M sodium phosphate pH 8.0 and 1 M ammonium

581   sulfate, with an 18 h incubation at 30°C. Beads were washed once with 100 mM Glycine pH 2.5,

582   once with 10 mM Tris pH 8.8, 4 times with PBS and twice with PBS plus 0.5% Triton X-100.

583   Beads were stored at -20°C in PBS with 50% glycerol.

584

585   **Mass spectrometry**

586   For immunoprecipitation, 4×10^6 832/13 cells were plated onto 10 cm petri dishes. Twenty-

587   four hours later, cells were transfected with either EIPR1::GFP or GFP. After 24 hours, cells were

588   washed with PBS and harvested in lysis buffer [50 mM Tris pH 7.5, 150 mM NaCl, 1% NP-40,

589   Protease inhibitor cocktail (Pierce)]. Lysates were passed 10 times through a 20G needle and

590   incubated for 30 min at 4°C. Lysates were pre-cleared by a 20,000 g centrifugation at 4°C for 15

591   minutes and the supernatant was incubated with 30 µg of anti-GFP nanobody bound to magnetic

592   beads, for two hours at 4°C. The beads were washed three times with 250 μL wash buffer (50 mM

593   Tris pH 7.5, 300 mM NaCl, 1% NP-40). Samples were eluted in two steps with (1) 0.2 M glycine

594   pH 2.5 and (2) 1 M NH4OH. Eluents were neutralized with 0.33 M Tris-HCl pH 7.5 and stored at -

595   80°C.

596   Samples were processed using modified FASP (filter aided sample preparation) to remove

597   mass spec incompatible substances (86). Samples were filtered with 10K Amicon Ultra 0.5 ml

598   filters (Millipore). Samples were buffer exchanged with 8 M urea in 50 mM ammonium bicarbonate

599   pH 7.8, reduced with TCEP (Pierce), alkylated with IAA (Sigma) and digested with trypsin (Pierce).

600   Samples were concentrated by speed vacuum.

601   A total of 0.15 μg of peptides was chromatographically separated onto a Thermo LTQ-

602   Velos Pro mass spectrometer coupled with a Waters nanoACQUITY liquid chromatography

603   system. A 75 μm fused silica column (Polymicro Technologies) was loaded with 30 cm C12

604   Jupiter (Phenomenex), 4 μm reverse-phase beads, and a 100 μm fused silica Kasil frit trap (PQ

605   Corporation) loaded with 4 cm of C12 Jupiter. Peptides were separated by a 110 minute gradient

606   consisting of buffer A (95% water, 5% acetonitrile and 0.1% formic acid) and buffer B (95%

607   acetonitrile, 5% water and 0.1% formic acid). Two analytical replicates were run for each sample

608   with each set of replicates randomized. Quality control samples were run every sixth sample and

609   at the beginning of the runs to assess column chromatography stability.

610   Data were searched with SEQUEST (87) against a *Rattus norvegicus* FASTA database

611   containing contaminants. False discovery rates were determined via a decoy database using

612   Percolator (88) at a q-value threshold of 0.01 and peptides were assembled into protein

613   identifications using ID Picker (89). Lists of EIPR1::GFP hits were assembled after first subtracting

614   hits found in a GFP control pulldown (Figure S5A) or subtracting hits found in the pulldowns of two

615   other proteins, CCCP1::GFP and RUNDC1::GFP (Figure S5B), performed in parallel.

616

617   **Coimmunoprecipitation and immunoblotting**

618   For co-immunoprecipitation, 832/13 cells were cultured and lysed as described above

619   (Mass spectrometry). The lysates were incubated with 20 μg anti-GFP nanobody bound to

620   magnetic beads, the beads were washed three times with lysis buffer and resuspended in

621   Laemmli loading buffer. Samples were resolved on 10% SDS-polyacrylamide gels and blotted

622   onto nitrocellulose or PVDF membranes. To detect co-precipitated proteins, we added the

623   following primary antibodies: mouse monoclonal anti-GFP (1:1000, Santa Cruz #sc-9996),

624   monoclonal anti-mCherry (1:50, a gift from Jihong Bai and the Fred Hutchinson Cancer Research

625   Center antibody development shared resource center), monoclonal anti-VPS50 (1:1000,

626   FLJ20097 monoclonal antibody, clone 2D11, Abnova #H00055610-M01), rabbit polyclonal anti-

627   SNAP29 (1:1000, Sigma #S2069), or monoclonal anti-beta-tubulin as a loading control (1:1000,

26

628 ThermoFisher, BT7R, #MA5-16308). The secondary antibody was an Alexa Fluor 680-conjugated

629 goat anti-mouse antibody (1:20,000, Jackson Laboratory #115-625-166) or Alexa Fluor 680-

630 conjugated goat anti-rabbit antibody (1:20,000, Jackson Laboratory #115-625-144). A LI-COR

631 processor was used to develop images.

632

633 **Imaging and image analysis**

634   Worms were mounted on 2% agarose pads and anesthetized with 50 mM sodium azide.

635 Images were obtained using a Nikon 80i wide-field compound microscope except for the images

636 shown in Fig 6A&B which were obtained on an Olympus confocal microscope, and the images in

637 Fig 6C&D which were obtained on a Deltavision deconvolution microscope. To image the dorsal

638 nerve cords, young adult animals were oriented with dorsal side up by exposure to the anesthetic

639 for ten minutes on the slide before placing the cover slip. For quantitative imaging of dorsal cord

640 fluorescence, all strains in a given experiment were imaged on the same days and all microscope

641 settings were kept constant. The same section of the dorsal cord around the vulva was imaged in

642 all worms. Maximum intensity projections were quantified using ImageJ software, measuring the

643 total fluorescence in a region of interest encapsulating the cord and subtracting the background

644 fluorescence of a region of identical size adjacent to the cord.

645

646 **Immunostaining of 832/13 cells**

647      $2x10^5$ 832/13 cells per well were seeded onto sterilized cover slips placed in 12 well cell

648 culture plates. The next day, cells were rinsed twice with ice-cold PBS and fixed with 4%

649 paraformaldehyde in PBS for 20 minutes at room temperature. The cells were rinsed twice with

650 PBS and permeabilized with 0.5% Triton X-100 in PBS for 5 minutes at room temperature. The

651 cells were again washed twice with PBS and then placed in 5% milk in PBS for 1 hour at room

652 temperature, followed by immunofluorescence staining with rabbit polyclonal anti-CCDC132 (1:50,

653 Sigma #HPA026679) and mouse monoclonal anti-GFP (1:350, Santa Cruz #sc-9996) in 0.5% milk

27

654 in PBS at room temperature for 1 hour. The cells were then washed with PBS three times for 5

655 minutes each, and incubated with Rhodamine anti-rabbit secondary antibody (1:1000, Jackson

656 Immunoresearch #111-025-144) and Alexa Fluor 488 anti-mouse secondary antibody (1:1000,

657 Jackson Immunoresearch #115-545-146) at room temperature for 1 hour. The cells were washed

658 with PBS three times for 5 min each and examined by fluorescence microscopy (Nikon 80i wide-

659 field compound microscope). The anti-CCDC132 antibody recognizes VPS50.

660

661 **Statistics**

662   P values were determined using GraphPad Prism 5.0d (GraphPad Software). Data sets

663 with multiple comparisons were analyzed by a one-way ANOVA followed by a Bonferroni posthoc

664 test to examine selected comparisons or by Dunnett's test if all comparisons were to the wild type

665 control. Pairwise data comparisons were analyzed by two-tailed unpaired t tests.

666

677

678 **References**

679

680 1. Borgonovo B, Ouwendijk J, Solimena M. Biogenesis of secretory granules. Curr Opin Cell
681   Biol. 2006 Aug;18(4):365–70.

682 2. Kim T, Gondré-Lewis MC, Arnaoutova I, Loh YP. Dense-core secretory granule biogenesis.
683   Physiology (Bethesda). 2006 Apr;21:124–33.

684 3. Park JJ, Loh YP. How peptide hormone vesicles are transported to the secretion site for
685   exocytosis. Mol Endocrinol. 2008 Dec;22(12):2583–95.

686 4. Tooze SA, Martens GJ, Huttner WB. Secretory granule biogenesis: rafting to the SNARE.
687   Trends Cell Biol. 2001 Mar;11(3):116–22.

688 5. Ahras M, Otto GP, Tooze SA. Synaptotagmin IV is necessary for the maturation of secretory
689   granules in PC12 cells. J Cell Biol. 2006 Apr 24;173(2):241–51.

690 6. Dittie AS, Hajibagheri N, Tooze SA. The AP-1 adaptor complex binds to immature secretory
691   granules from PC12 cells, and is regulated by ADP-ribosylation factor. J Cell Biol. 1996
692   Feb;132(4):523–36.

693 7. Kakhlon O, Sakya P, Larijani B, Watson R, Tooze SA. GGA function is required for
694   maturation of neuroendocrine secretory granules. EMBO J. 2006 Apr 19;25(8):1590–602.

695 8. Klumperman J, Kuliawat R, Griffith JM, Geuze HJ, Arvan P. Mannose 6-phosphate receptors
696   are sorted from immature secretory granules via adaptor protein AP-1, clathrin, and syntaxin
697   6-positive vesicles. J Cell Biol. 1998 Apr 20;141(2):359–71.

698 9. Tooze SA, Flatmark T, Tooze J, Huttner WB. Characterization of the immature secretory
699   granule, an intermediate in granule biogenesis. J Cell Biol. 1991 Dec;115(6):1491–503.

700 10. Urbé S, Page LJ, Tooze SA. Homotypic fusion of immature secretory granules during
701   maturation in a cell-free assay. J Cell Biol. 1998 Dec 28;143(7):1831–44.

702 11. Wendler F, Page L, Urbé S, Tooze SA. Homotypic fusion of immature secretory granules
703   during maturation requires syntaxin 6. Mol Biol Cell. 2001 Jun;12(6):1699–709.

704 12. Chanat E, Huttner WB. Milieu-induced, selective aggregation of regulated secretory proteins
705   in the trans-Golgi network. J Cell Biol. 1991 Dec;115(6):1505–19.

706 13. Dikeakos JD, Reudelhuber TL. Sending proteins to dense core secretory granules: still a lot
707   to sort out. J Cell Biol. 2007 Apr 23;177(2):191–6.

708 14. Dikeakos JD, Di Lello P, Lacombe M-J, Ghirlando R, Legault P, Reudelhuber TL, et al.
709   Functional and structural characterization of a dense core secretory granule sorting domain
710   from the PC1/3 protease. Proc Natl Acad Sci USA. 2009 May 5;106(18):7408–13.

711 15. Arvan P, Castle D. Sorting and storage during secretory granule biogenesis: looking
712   backward and looking forward. Biochem J. 1998 Jun 15;332 (Pt 3):593–610.

29

16. Tooze SA. Biogenesis of secretory granules in the trans-Golgi network of neuroendocrine and endocrine cells. Biochim Biophys Acta. 1998 Aug 14;1404(1-2):231–44.

17. Buffa L, Fuchs E, Pietropaolo M, Barr F, Solimena M. ICA69 is a novel Rab2 effector regulating ER-Golgi trafficking in insulinoma cells. Eur J Cell Biol. 2008 Apr;87(4):197–209.

18. Cao M, Mao Z, Kam C, Xiao N, Cao X, Shen C, et al. PICK1 and ICA69 control insulin granule trafficking and their deficiencies lead to impaired glucose tolerance. PLoS Biol. 2013;11(4):e1001541.

19. Edwards SL, Charlie NK, Richmond JE, Hegermann J, Eimer S, Miller KG. Impaired dense core vesicle maturation in Caenorhabditis elegans mutants lacking Rab2. J Cell Biol. 2009 Sep 21;186(6):881–95.

20. Hannemann M, Sasidharan N, Hegermann J, Kutscher LM, Koenig S, Eimer S. TBC-8, a putative RAB-2 GAP, regulates dense core vesicle maturation in Caenorhabditis elegans. PLoS Genet. 2012;8(5):e1002722.

21. Holst B, Madsen KL, Jansen AM, Jin C, Rickhag M, Lund VK, et al. PICK1 deficiency impairs secretory vesicle biogenesis and leads to growth retardation and decreased glucose tolerance. PLoS Biol. 2013;11(4):e1001542.

22. Sumakovic M, Hegermann J, Luo L, Husson SJ, Schwarze K, Olendrowitz C, et al. UNC-108/RAB-2 and its effector RIC-19 are involved in dense core vesicle maturation in Caenorhabditis elegans. J Cell Biol. 2009 Sep 21;186(6):897–914.

23. Ailion M, Hannemann M, Dalton S, Pappas A, Watanabe S, Hegermann J, et al. Two Rab2 interactors regulate dense-core vesicle maturation. Neuron. 2014 Apr 2;82(1):167–80.

24. Li C, Kim K, Nelson LS. FMRFamide-related neuropeptide gene family in Caenorhabditis elegans. Brain Res. 1999 Nov 27;848(1-2):26–34.

25. Nathoo AN, Moeller RA, Westlund BA, Hart AC. Identification of neuropeptide-like protein gene families in Caenorhabditiselegans and other species. Proc Natl Acad Sci USA. 2001 Nov 20;98(24):14000–5.

26. Pierce SB, Costa M, Wisotzkey R, Devadhar S, Homburger SA, Buchman AR, et al. Regulation of DAF-2 receptor signaling by human insulin and *ins-1*, a member of the unusually large and diverse C. elegans insulin gene family. Genes Dev. 2001 Mar 15;15(6):672–86.

27. Cai T, Fukushige T, Notkins AL, Krause M. Insulinoma-Associated Protein IA-2, a Vesicle Transmembrane Protein, Genetically Interacts with UNC-31/CAPS and Affects Neurosecretion in Caenorhabditis elegans. J Neurosci. 2004 Mar 24;24(12):3115–24.

28. Stirnimann CU, Petsalaki E, Russell RB, Müller CW. WD40 proteins propel cellular networks. Trends Biochem Sci. 2010 Oct;35(10):565–74.

29. Gondré-Lewis MC, Park JJ, Loh YP. Cellular mechanisms for the biogenesis and transport of synaptic and dense-core vesicles. Int Rev Cell Mol Biol. 2012;299:27–115.

30. Hou JC, Min L, Pessin JE. Insulin granule biogenesis, trafficking and exocytosis. Vitam Horm. 2009;80:473–506.

31. Bonifacino JS, Hierro A. Transport according to GARP: receiving retrograde cargo at the trans-Golgi network. Trends Cell Biol. 2011 Mar;21(3):159–67.

32. Gillingham AK, Sinka R, Torres IL, Lilley KS, Munro S. Toward a comprehensive map of the effectors of rab GTPases. Dev Cell. 2014 Nov 10;31(3):358–73.

33. Schindler C, Chen Y, Pu J, Guo X, Bonifacino JS. EARP is a multisubunit tethering complex involved in endocytic recycling. Nat Cell Biol. 2015 May;17(5):639–50.

34. Luo L, Hannemann M, Koenig S, Hegermann J, Ailion M, Cho M-K, et al. The Caenorhabditis elegans GARP complex contains the conserved Vps51 subunit and is required to maintain lysosomal morphology. Mol Biol Cell. 2011 Jul 15;22(14):2564–78.

35. Sieburth D, Madison JM, Kaplan JM. PKC-1 regulates secretion of neuropeptides. Nat Neurosci. 2007 Jan;10(1):49–57.

36. Speese S, Petrie M, Schuske K, Ailion M, Ann K, Iwasaki K, et al. UNC-31 (CAPS) is required for dense-core vesicle but not synaptic vesicle exocytosis in Caenorhabditis elegans. J Neurosci. 2007 Jun 6;27(23):6150–62.

37. Hein MY, Hubner NC, Poser I, Cox J, Nagaraj N, Toyoda Y, et al. A human interactome in three quantitative dimensions organized by stoichiometries and abundances. Cell. 2015 Oct 22;163(3):712–23.

38. Huttlin EL, Ting L, Bruckner RJ, Gebreab F, Gygi MP, Szpyt J, et al. The BioPlex Network: A Systematic Exploration of the Human Interactome. Cell. 2015 Jul 16;162(2):425–40.

39. Wan C, Borgeson B, Phanse S, Tu F, Drew K, Clark G, et al. Panorama of ancient metazoan macromolecular complexes. Nature. 2015 Sep 17;525(7569):339–44.

40. Hu RJ, Lee MP, Connors TD, Johnson LA, Burn TC, Su K, et al. A 2.5-Mb transcript map of a tumor-suppressing subchromosomal transferable fragment from 11p15.5, and isolation and sequence analysis of three novel genes. Genomics. 1997 Nov 15;46(1):9–17.

41. Hirst J, Barlow LD, Francisco GC, Sahlender DA, Seaman MNJ, Dacks JB, et al. The fifth adaptor protein complex. PLoS Biol. 2011 Oct;9(10):e1001170.

42. Kang J, Bai Z, Zegarek MH, Grant BD, Lee J. Essential roles of snap-29 in C. elegans. Dev Biol. 2011 Jul 1;355(1):77–88.

43. Morelli E, Ginefra P, Mastrodonato V, Beznoussenko GV, Rusten TE, Bilder D, et al. Multiple functions of the SNARE protein Snap29 in autophagy, endocytic, and exocytic trafficking during epithelial formation in Drosophila. Autophagy. 2014;10(12):2251–68.

44. Rapaport D, Lugassy Y, Sprecher E, Horowitz M. Loss of SNAP29 impairs endocytic recycling and cell motility. PLoS ONE. 2010;5(3):e9759.

45. Sato M, Saegusa K, Sato K, Hara T, Harada A, Sato K. Caenorhabditis elegans SNAP-29 is required for organellar integrity of the endomembrane system and general exocytosis in intestinal epithelial cells. Mol Biol Cell. 2011 Jul 15;22(14):2579–87.

46. Conibear E, Cleck JN, Stevens TH. Vps51p mediates the association of the GARP (Vps52/53/54) complex with the late Golgi t-SNARE Tlg1p. Mol Biol Cell. 2003 Apr;14(4):1610–23.

47. Perez-Victoria FJ, Schindler C, Magadan JG, Mardones GA, Delevoye C, Romao M, et al. Ang2/Fat-Free Is a Conserved Subunit of the Golgi-associated Retrograde Protein Complex. Mol Biol Cell. 2010 Oct 1;21(19):3386–95.

48. Pérez-Victoria FJ, Bonifacino JS. Dual roles of the mammalian GARP complex in tethering and SNARE complex assembly at the trans-golgi network. Mol Cell Biol. 2009 Oct;29(19):5251–63.

49. Siniossoglou S, Pelham HR. An effector of Ypt6p binds the SNARE Tlg1p and mediates selective fusion of vesicles with late Golgi membranes. EMBO J. 2001 Nov 1;20(21):5991–8.

50. Conibear E, Stevens TH. Vps52p, Vps53p, and Vps54p form a novel multisubunit complex required for protein sorting at the yeast late Golgi. Mol Biol Cell. 2000 Jan;11(1):305–23.

51. Pérez-Victoria FJ, Mardones GA, Bonifacino JS. Requirement of the human GARP complex for mannose 6-phosphate-receptor-dependent sorting of cathepsin D to lysosomes. Mol Biol Cell. 2008 Jun;19(6):2350–62.

52. Fröhlich F, Petit C, Kory N, Christiano R, Hannibal-Bach H-K, Graham M, et al. The GARP complex is required for cellular sphingolipid homeostasis. Elife. 2015;4.

53. Hirata T, Fujita M, Nakamura S, Gotoh K, Motooka D, Murakami Y, et al. Post-Golgi anterograde transport requires GARP-dependent endosome-to-TGN retrograde transport. Mol Biol Cell. 2015 Sep 1;26(17):3071–84.

54. Matsumoto Y, Imai Y, Sugita Y, Tanaka T, Tsujimoto G, Saito H, et al. CCDC132 is highly expressed in atopic dermatitis T cells. Mol Med Rep. 2010 Feb;3(1):83–7.

55. Paquin N, Murata Y, Froehlich A, Omura D, Ailion M, Pender C, et al. The conserved VPS-50 protein functions in dense-core vesicle maturation and acidification and controls animal behavior. Curr Biol. 2016 doi:10.1016/j.cub.2016.01.049

56. McCall RD. HPNS seizure risk: a role for the Golgi-associated retrograde protein complex? Undersea Hyperb Med. 2011 Feb;38(1):3–9.

57. Schmitt-John T, Drepper C, Mussmann A, Hahn P, Kuhlmann M, Thiel C, et al. Mutation of Vps54 causes motor neuron disease and defective spermiogenesis in the wobbler mouse. Nat Genet. 2005 Nov;37(11):1213–5.

58. Feinstein M, Flusser H, Lerman-Sagie T, Ben-Zeev B, Lev D, Agamy O, et al. VPS53 mutations cause progressive cerebello-cerebral atrophy type 2 (PCCA2). J Med Genet. 2014 May;51(5):303–8.

59. Bäck N, Rajagopal C, Mains RE, Eipper BA. Secretory granule membrane protein recycles through multivesicular bodies. Traffic. 2010 Jul 1;11(7):972–86.

60. Sobota JA, Ferraro F, Bäck N, Eipper BA, Mains RE. Not all secretory granules are created equal: Partitioning of soluble content proteins. Mol Biol Cell. 2006 Dec;17(12):5038–52.

61. Mesa R, Luo S, Hoover CM, Miller K, Minniti A, Inestrosa N, et al. HID-1, a New Component of the Peptidergic Signaling Pathway. Genetics. 2011 Feb;187(2):467–83.

62. Yu Y, Wang L, Jiu Y, Zhan Y, Liu L, Xia Z, et al. HID-1 is a novel player in the regulation of neuropeptide sorting. Biochem J. 2011 Feb 24;434(3):383–90.

63. Gehart H, Goginashvili A, Beck R, Morvan J, Erbs E, Formentini I, et al. The BAR domain protein Arfaptin-1 controls secretory granule biogenesis at the trans-Golgi network. Dev Cell. 2012 Oct 16;23(4):756–68.

64. Pinheiro PS, Jansen AM, de Wit H, Tawfik B, Madsen KL, Verhage M, et al. The BAR domain protein PICK1 controls vesicle number and size in adrenal chromaffin cells. J Neurosci. 2014 Aug 6;34(32):10688–700.

65. Torres IL, Rosa-Ferreira C, Munro S. The Arf family G protein Arl1 is required for secretory granule biogenesis in Drosophila. J Cell Sci. 2014 May 15;127(Pt 10):2151–60.

66. Asensio CS, Sirkis DW, Edwards RH. RNAi screen identifies a role for adaptor protein AP-3 in sorting to the regulated secretory pathway. J Cell Biol. 2010 Dec 13;191(6):1173–87.

67. Bonnemaison M, Bäck N, Lin Y, Bonifacino JS, Mains R, Eipper B. AP-1A controls secretory granule biogenesis and trafficking of membrane secretory granule proteins. Traffic. 2014 Oct;15(10):1099–121.

68. Burgess J, Jauregui M, Tan J, Rollins J, Lallet S, Leventis PA, et al. AP-1 and clathrin are essential for secretory granule biogenesis in Drosophila. Mol Biol Cell. 2011 Jun;22(12):2094–105.

69. Sirkis DW, Edwards RH, Asensio CS. Widespread dysregulation of peptide hormone release in mice lacking adaptor protein AP-3. PLoS Genet. 2013;9(9):e1003812.

70. Asensio CS, Sirkis DW, Maas JW Jr, Egami K, To T-L, Brodsky FM, et al. Self-assembly of VPS41 promotes sorting required for biogenesis of the regulated secretory pathway. Dev Cell. 2013 Nov 25;27(4):425–37.

71. Chen X-W, Feng Y-Q, Hao C-J, Guo X-L, He X, Zhou Z-Y, et al. DTNBP1, a schizophrenia susceptibility gene, affects kinetics of transmitter release. J Cell Biol. 2008 Jun 2;181(5):791–801.

72. Hao Z, Wei L, Feng Y, Chen X, Du W, Ma J, et al. Impaired maturation of large dense-core vesicles in muted-deficient adrenal chromaffin cells. J Cell Sci. 2015 Apr 1;128(7):1365–74.

73. Briguglio JS, Kumar S, Turkewitz AP. Lysosomal sorting receptors are essential for secretory granule biogenesis in Tetrahymena. J Cell Biol. 2013 Nov 11;203(3):537–50.

74. Kebede MA, Oler AT, Gregg T, Balloon AJ, Johnson A, Mitok K, et al. SORCS1 is necessary for normal insulin secretory granule biogenesis in metabolically stressed β cells. J Clin Invest. 2014 Oct;124(10):4240–56.

75. Robinson MS. Adaptable adaptors for coated vesicles. Trends Cell Biol. 2004 Apr;14(4):167–74.

76. Walter AM, Kurps J, de Wit H, Schöning S, Toft-Bertelsen TL, Lauks J, et al. The SNARE protein vti1a functions in dense-core vesicle biogenesis. EMBO J. 2014 Aug 1;33(15):1681–97.

77. Bock JB, Klumperman J, Davanger S, Scheller RH. Syntaxin 6 functions in trans-Golgi network vesicle trafficking. Mol Biol Cell. 1997 Jul;8(7):1261–71.

78. Frøkjaer-Jensen C, Davis MW, Hopkins CE, Newman BJ, Thummel JM, Olesen S-P, et al. Single-copy insertion of transgenes in Caenorhabditis elegans. Nat Genet. 2008 Nov;40(11):1375–83.

79. Frøkjær-Jensen C, Davis MW, Ailion M, Jorgensen EM. Improved Mos1-mediated transgenesis in C. elegans. Nat Methods. 2012 Feb;9(2):117–8.

80. Mello CC, Kramer JM, Stinchcomb D, Ambros V. Efficient gene transfer in C.elegans: extrachromosomal maintenance and integration of transforming sequences. EMBO J. 1991 Dec;10(12):3959–70.

81. Dickinson DJ, Ward JD, Reiner DJ, Goldstein B. Engineering the Caenorhabditis elegans genome using Cas9-triggered homologous recombination. Nat Methods. 2013 Oct;10(10):1028–34.

82. Miller KG, Emerson MD, Rand JB. Goalpha and diacylglycerol kinase negatively regulate the Gqalpha pathway in C. elegans. Neuron. 1999 Oct;24(2):323–33.

83. Hohmeier HE, Mulder H, Chen G, Henkel-Rieger R, Prentki M, Newgard CB. Isolation of INS-1-derived cell lines with robust ATP-sensitive K+ channel-dependent and -independent glucose-stimulated insulin secretion. Diabetes. 2000 Mar 1;49(3):424–30.

84. Fridy PC, Li Y, Keegan S, Thompson MK, Nudelman I, Scheid JF, et al. A robust pipeline for rapid production of versatile nanobody repertoires. Nat Methods. 2014 Dec;11(12):1253–60.

85. Skerra A, Plückthun A. Assembly of a functional immunoglobulin Fv fragment in Escherichia coli. Science. 1988 May 20;240(4855):1038–41.

86. Wiśniewski JR, Zougman A, Nagaraj N, Mann M. Universal sample preparation method for proteome analysis. Nat Methods. 2009 May;6(5):359–62.

87. Eng JK, McCormack AL, Yates JR. An approach to correlate tandem mass spectral data of peptides with amino acid sequences in a protein database. J Am Soc Mass Spectrom. 1994 Nov;5(11):976–89.

88. Käll L, Canterbury JD, Weston J, Noble WS, MacCoss MJ. Semi-supervised learning for peptide identification from shotgun proteomics datasets. Nat Methods. 2007 Nov;4(11):923–5.

89. Zhang B, Chambers MC, Tabb DL. Proteomic parsimony through bipartite graph analysis improves accuracy and transparency. J Proteome Res. 2007 Sep;6(9):3549–57.

900 **Supporting information captions**

901

902 **S1 Figure. *eipr-1* mutants have egg laying defects.**

903 (A) *eipr-1* acts in neurons to control egg laying. The graph shows the number of eggs laid by 5

904 animals in a 2.5 hour period. *eipr-1* mutants show egg-laying defects and this phenotype is

905 rescued by panneuronal expression of either the worm gene or its mouse ortholog (***, P<0.001).

906 Error bars = SEM; n =10 plates of 5 worms each.

907 (B) *eipr-1* acts in the same pathway as *rab-2* to control egg-laying. Double mutants of *eipr-1* with

908 *rab-2* or *rund-1* do not have stronger egg-laying defects than the single mutants. Though *rund-1*

909 mutants have a visible Egl (egg-laying defective) phenotype indicating that they retain more eggs,

910 they did not have a significantly reduced egg-laying rate as measured by this assay. Error bars =

911 SEM; n = 5 plates of 5 worms each. ns, not significant, P>0.05.

912

913 **S2 Figure. Alignment of EIPR-1.** Alignment of *C. elegans* EIPR-1 (worm, accession #

914 NP_493383.1) and its orthologs from *Arabidopsis thaliana* (Arabidopsis, accession #

915 NP_173478.2), *Drosophila melanogaster* (fly, CG10646, accession # NP_648581.1), and *Homo*

916 *sapiens* (human, TSSC1, accession # NP_003301.1). Identical residues are shaded in black and

917 similar residues are shaded in gray. The WD40 repeats (from SMART, using the worm protein;

918 http://smart.embl-heidelberg.de/) are marked with single black bars. Using SMART, worm EIPR-1

919 has four predicted WD40 repeats, Arabidopsis has six, fly has three, and human has five. WD40

920 repeats are difficult to identify by primary sequence and are often missed by prediction programs.

921 The position of the ox316 stop mutation is marked with an asterisk. Alignment was made with

922 MUSCLE (http://www.ebi.ac.uk/Tools/msa/muscle/) using default parameters and exhibited with

923 Boxshade 3.21 (http://www.ch.embnet.org/software/BOX_form.html).

924

35

925 **S3 Figure. *eipr-1* mutants have defects in trafficking dense-core vesicle cargos but not**

926 **synaptic vesicle cargos.**

927 (A) Representative images of FLP-3::Venus fluorescence in dorsal cord motor neuron axons of

928 the wild type and *eipr-1(tm4790)* mutant strains. Scale bar: 10 µm. *eipr-1* mutants have decreased

929 fluorescence in the dorsal cord, indicative of a FLP-3::Venus sorting or trafficking defect.

930 (B) Representative images of INS-22::Venus fluorescence in dorsal cord motor neuron axons.

931 Scale bar: 10 µm.

932 (C) Representative images of IDA-1::GFP fluorescence in the dorsal nerve cord. Scale bar: 10

933 µm.

934 (D) SNB-1::GFP fluorescence levels in the dorsal nerve cord. *eipr-1* mutants do not have a defect

935 (ns = not significant, P>0.05). Error bars = SEM; n =21-26.

936

937 **S4 Figure. Expression and localization of EIPR-1.**

938 (A) Representative images of animals expressing GFP under the promoter region upstream of the

939 first gene (W09C5.1) of the operon where *eipr-1* is located. The image on the left shows

940 expression in the hypodermis (skin) while the image on the right shows expression in the pharynx.

941 (B) Representative images of neurons expressing *eipr-1*::GFP under panneuronal (Left panel, *rab-*

942 *3p*) and head cholinergic (Right panel, *unc-17Hp*) promoters. Scale bars: 5 µm.

943 (C) Representative images of neurons coexpressing *rab-3p::eipr-1::*GFP and GTP-bound RAB-2

944 (RAB-2QL). Scale bars: 5 µm.

945

946 **S5 Figure. EIPR-1 interacts with members of the GARP and EARP complexes.**

947 List of top hits from two independent experiments (A, B) performing mass spectrometry of a

948 pulldown of rEIPR1::GFP in 832/13 cells. In A, we show the list of hits found after subtracting hits

949 found in a GFP control pulldown. In B, we show the list of hits found after subtracting hits found in

950 either the pulldown of CCCP1::GFP or RUNDC1::GFP. In both cases, EIPR1::GFP pulldowns

951   were performed in parallel to controls. # seq = number of unique peptides from each protein. All

952   proteins with two or more unique peptides are shown.

953

954   **S6 Figure. *vps-51* mutants have defects in trafficking FLP-3::Venus.**

955   FLP-3::Venus fluorescence levels in the dorsal nerve cord of wild type and *vps-51* mutant strains.

956   *vps-51* mutants have decreased fluorescence in the dorsal cord. Error bars = SEM; n = 8.

957

958   **S7 Figure. EARP, not GARP, is important for locomotion and trafficking dense-core vesicle**

959   **cargos.**

960   (A). GARP mutants *vps-54(ok1463)* and *vps-54(ok1473)* do not have a reduced locomotion rate.

961   Error bars = SEM; n = 10.

962   (B) *vps-50* acts in the same genetic pathway as *eipr-1* to control FLP-3::Venus trafficking. Left:

963   representative images. Right: quantification. *vps-50* and *eipr-1* have reduced FLP-3::Venus

964   fluorescence, but an *eipr-1; vps-50* double mutant does not have a stronger phenotype than either

965   single mutant indicating that *eipr-1* and *vps-50* act in the same genetic pathway. A *vps-54* mutant

966   does not have decreased axonal levels of FLP-3::Venus. ***, P<0.001 compared to wild type.

967   Error bars = SEM; n =9-14.

968   (C) *vps-50* mutants do not have defects in trafficking synaptic vesicle cargos. SNB-1::mCherry

969   fluorescence levels were measured in the dorsal nerve cord. ns, not significant, P>0.05 compared

970   to wild type. Error bars = SEM; n =11-14.

971

972   **S8 Figure. VPS50 partially colocalizes with RAB2 and CCCP1.**

973   (A) Representative images of 832/13 cells expressing GFP::RAB2A and costained for

974   endogenous VPS50. Scale bar: 10 μm.

975   (B) Representative images of 832/13 cells expressing CCCP1::GFP and costained for

976   endogenous VPS50. Scale bar: 10 μm.

977

S9 Figure. *eipr-1* and GARP/EARP mutants have reduced secretion of NLP-21::Venus.

NLP-21::Venus fluorescence levels in the coelomocytes of the indicated strains. Like *rab-2*

mutants*, eipr-1, vps-50,* and *vps-52* mutants show reductions in the accumulation of Venus

fluorescence in coelomocytes that is approximately proportional to the decrease in axonal

fluorescence seen in these mutants, suggesting that these mutants are not defective in dense-

core vesicle release. Double mutants between *eipr-1* and *rab-2* or *vps-50* do not have stronger

phenotypes than the single mutants, suggesting that these genes all act in the same dense-core

vesicle cargo sorting pathway. **, $P<0.01$; ***, $P<0.001$ compared to WT. Error bars = SEM; n =

14-33.

S10 Figure. *eipr-1* and *vps-50* mutants do not have enlarged lysosomes.

Representative images of LMP-1::GFP fluorescence in coelomocytes of WT, *eipr-1(tm4790)* and

vps-50(ok2627) mutant strains. Scale bar: 10 μm.

S11 Figure. VPS-52 localizes normally in *eipr-1* mutants.

Representative images of WT and *eipr-1(tm4790)* mutant neurons expressing VPS-52::tagRFP.

Scale bars: 1μm.

S12 Figure. EIPR-1 interacts with SNAP29.

EGFP-tagged rat EIPR1 or EGFP was expressed in 832/13 cells. Immunoprecipitation of

EIPR1::EGFP pulled down more SNAP29 than untagged EGFP. IN: input; IP:

immunoprecipitation.

S1 Table. List of strains.

1003 **S2 Table. List of plasmids.**

Figure 1

A

B

C

D
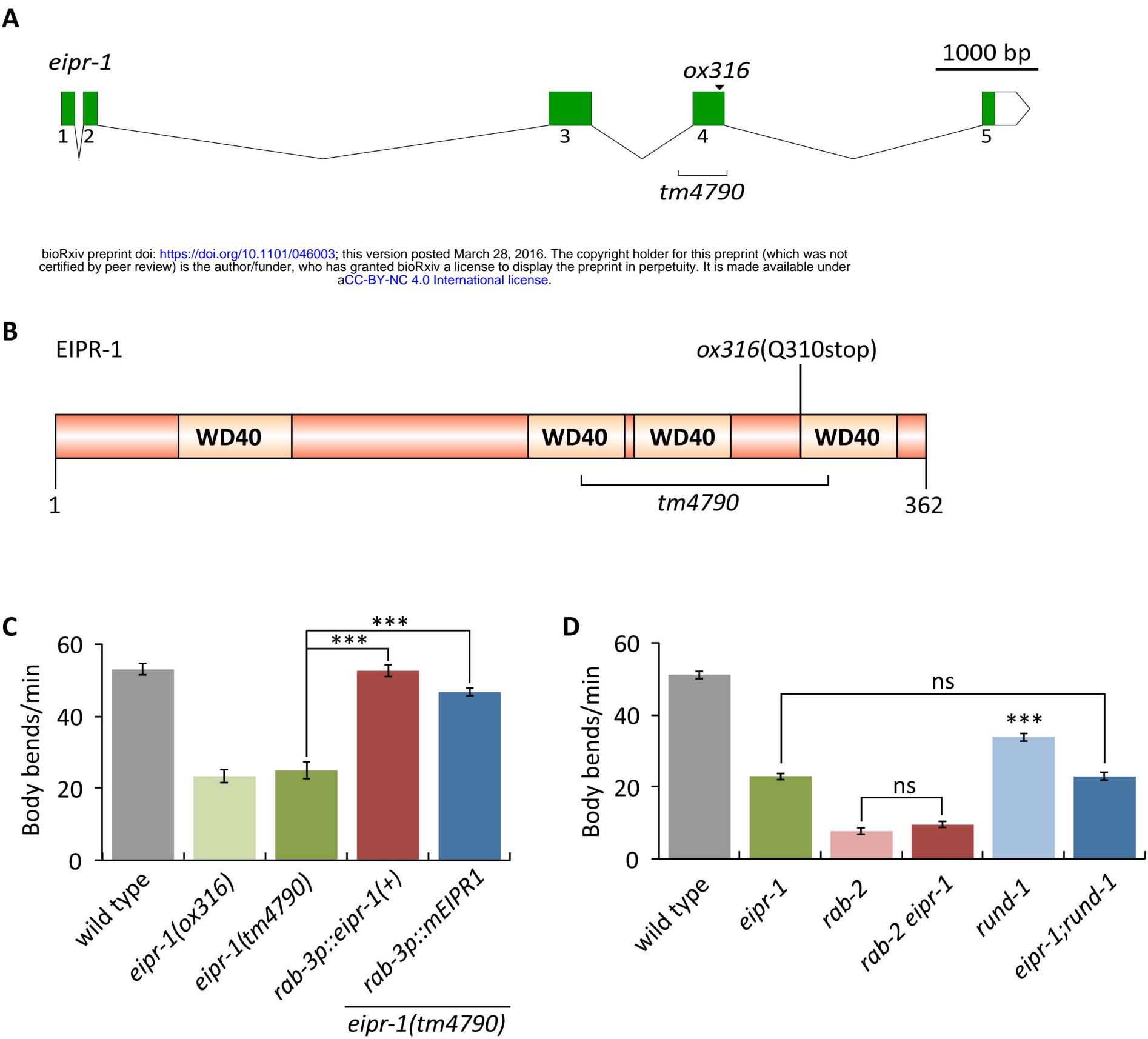
Figure 1. *eipr-1* encodes a WD40 domain protein that controls locomotion behavior.

(A) Gene structure of *eipr-1*. Solid boxes show coding segments. A white box shows the 3' untranslated region. The positions of the *ox316* stop mutation and the *tm4790* deletion are shown. The gene structures were drawn using Exon-Intron Graphic Maker (http://wormweb.org/exonintron).

(B) Domain structure of the EIPR-1 protein. EIPR-1 is a 362 amino acid protein with four predicted WD40 repeats. The part of the protein deleted by *tm4790* is marked, but because this deletion starts and ends in introns (Figure 1A), its precise effect on the protein is unknown, though it would cause a frameshift if exon 3 splices to exon 5 in this mutant. The protein structure was drawn using DOG 1.0 (Ren et al., 2009). WD40 repeat positions were as predicted by SMART (http://smart.embl-heidelberg.de/).

(C) *eipr-1* acts in neurons to control locomotion. The *eipr-1* mutant has slow locomotion that is rescued by panneuronal expression of either the worm gene or its mouse ortholog (***, P<0.001). Error bars = SEM; n = 10.

(D) *eipr-1* acts in the same genetic pathway as *rab-2* and *rund-1* to control locomotion. Double mutants of *eipr-1* with *rab-2* or *rund-1* do not have stronger locomotion defects than the single mutants (***, P<0.001 compared to wild type; ns, not significant, P>0.05). Error bars = SEM; n = 10.

Figure 2

A

NLP-21::Venus

B FLP-3::Venus

C INS-22::Venus

D IDA-1::GFP

UNC-17::GFP

**E**

F
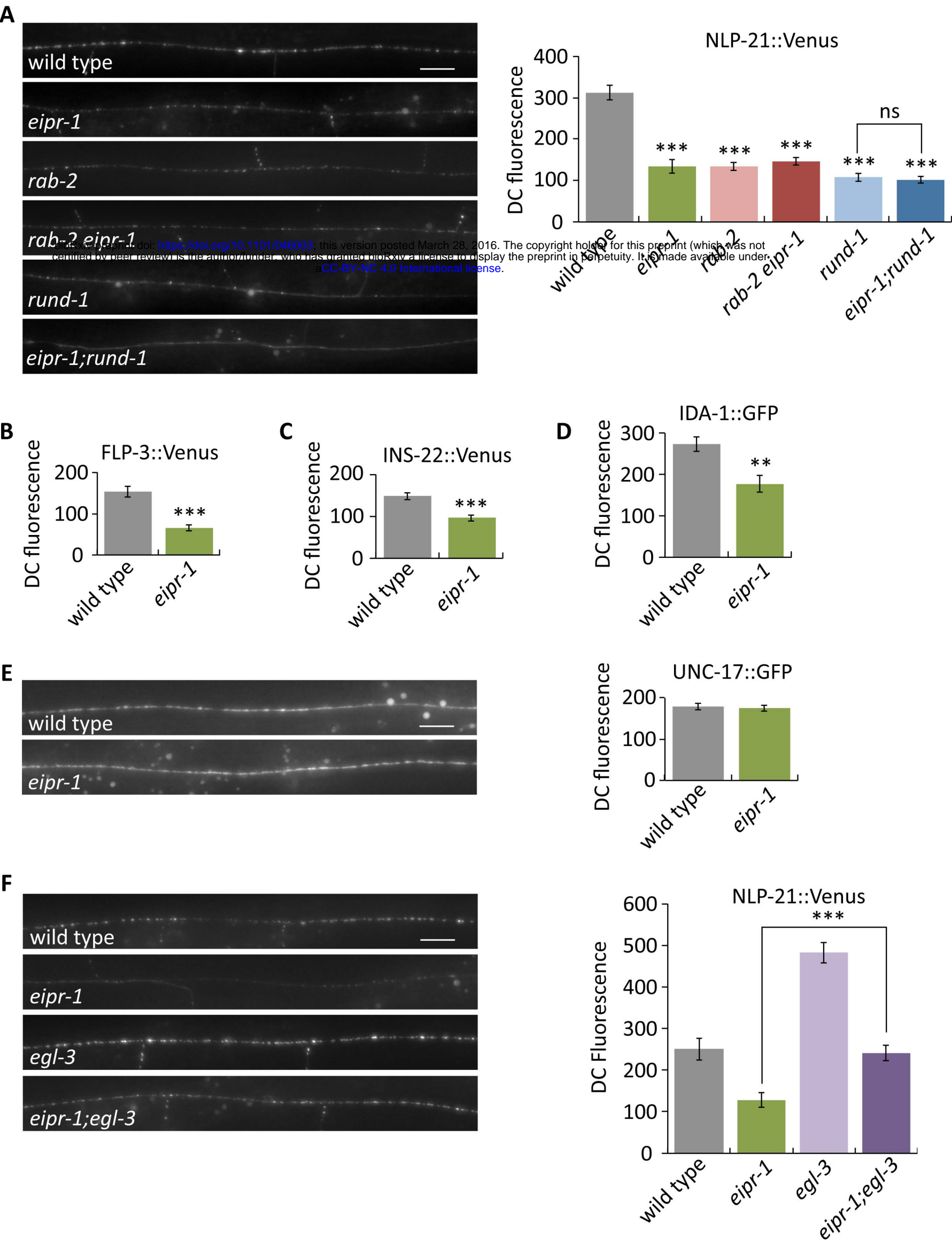
NLP-21::Venus

Figure 2. *eipr-1* mutants have defects in trafficking dense-core vesicle cargos.

(A) Left: representative images of NLP-21::Venus fluorescence in motor neuron axons of the dorsal nerve cord. Scale bar: 10 µm. Right: quantification of NLP-21::Venus fluorescence levels in the dorsal nerve cord. The mean fluorescence intensity is given in arbitrary units. *eipr-1, rab-2,* and *rund-1* mutants have decreased levels of fluorescence in the dorsal cord (DC), indicative of an NLP-21::Venus sorting or trafficking defect (***, P<0.001 compared to wild type). Double mutants of *eipr-1* with *rab-2* or *rund-1* are not significantly different than the single mutants (P>0.05). Error bars = SEM; n = 10.

(B) FLP-3::Venus fluorescence levels in the dorsal nerve cord. ***, P<0.001. Error bars = SEM; n = 12.

(C) INS-22::Venus fluorescence levels in the dorsal nerve cord. ***, P<0.001. Error bars = SEM; n = 11-12.

(D) IDA-1::GFP fluorescence levels in the dorsal nerve cord. **, P<0.01. Error bars = SEM; n = 13-14.

(E) UNC-17::GFP fluorescence levels in the dorsal nerve cord. *eipr-1* mutants do not have a defect (P>0.05). Scale bar: 10 µm. Error bars = SEM; n = 16-19.

(F) The peptide processing mutant *egl-3* increases the level of NLP-21::Venus in the dorsal cord in both wild type and *eipr-1* mutant backgrounds. Left: representative images. Scale bar: 10 µm. Right: quantification of NLP-21::Venus fluorescence levels in the dorsal nerve cord. ***, P<0.001. Error bars = SEM; n = 9-12.
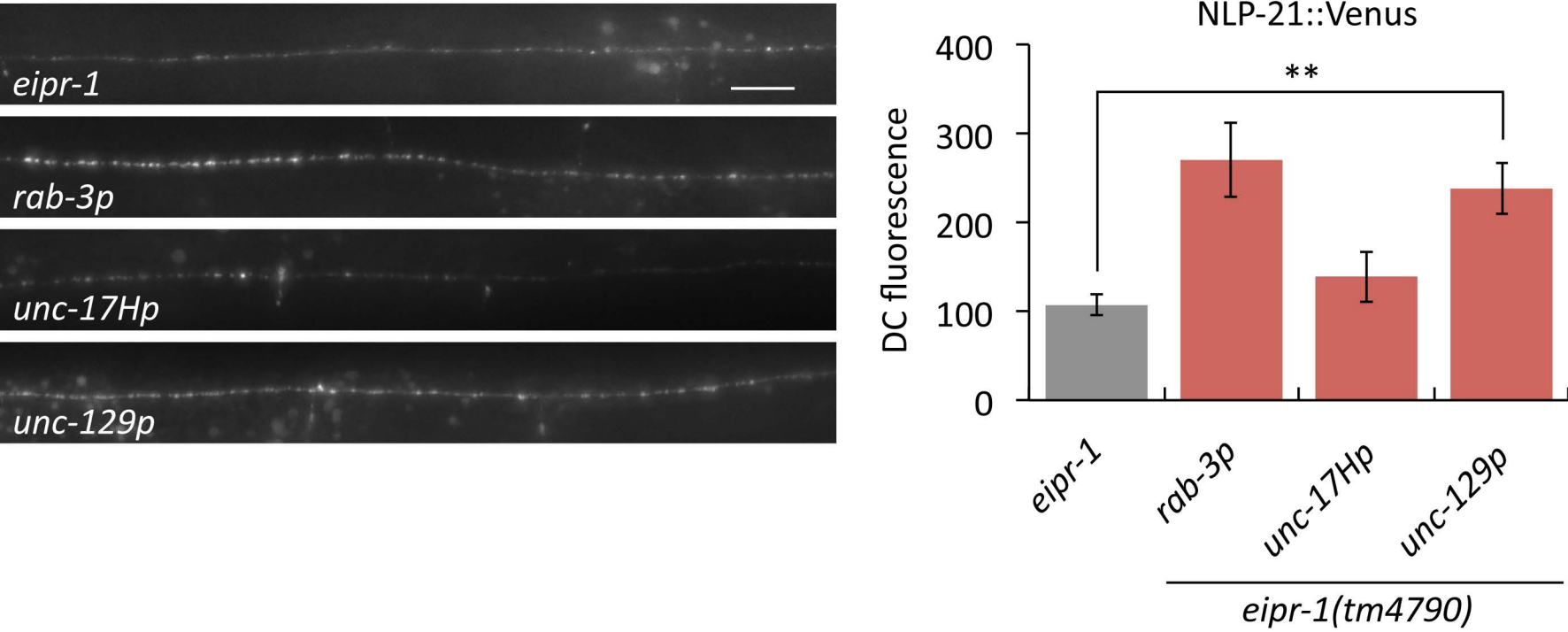
Figure 3

A
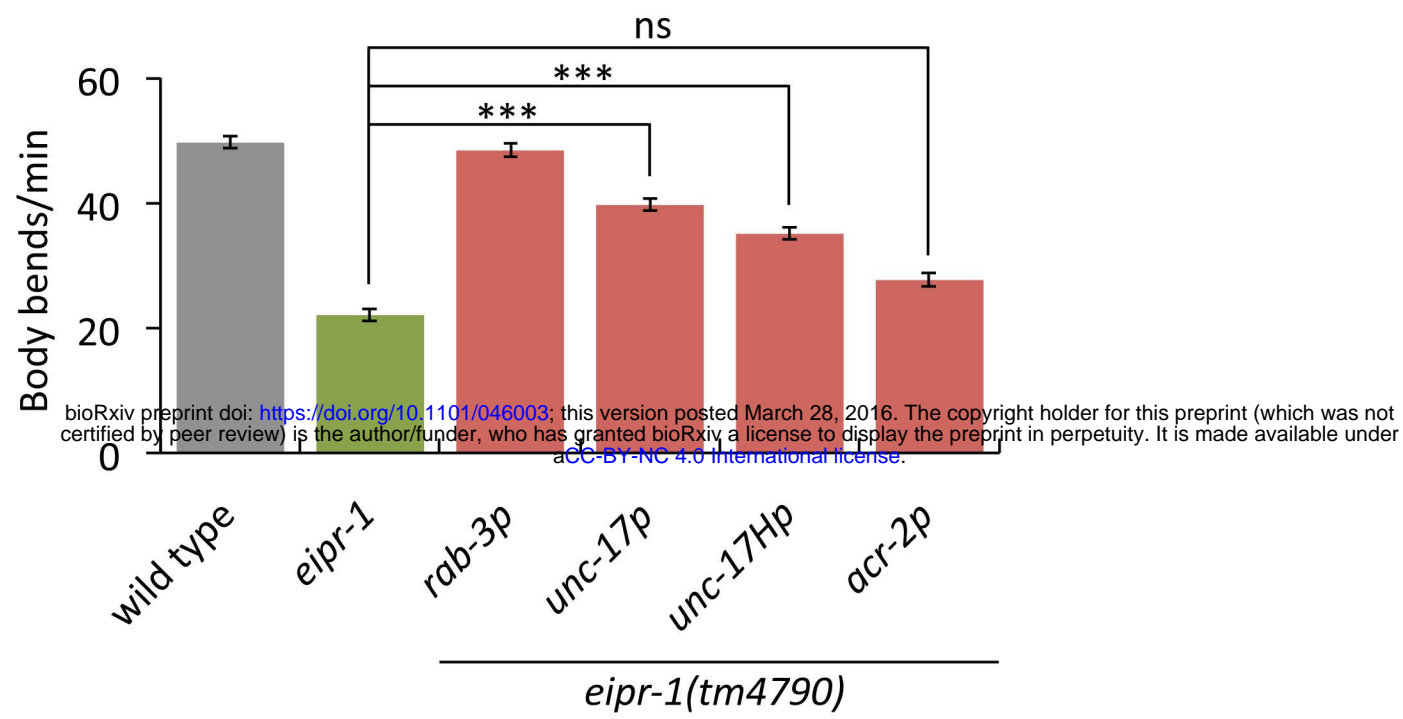
B

Figure 3. *eipr-1* acts in head cholinergic neurons to control locomotion.

(A) The *eipr-1* cDNA was expressed in an *eipr-1* mutant background using the following promoters: *rab-3* (all neurons), *unc-17* (cholinergic neurons), *unc-17H* (a derivative of the *unc-17* promoter that lacks the enhancer for ventral cord expression and thus expresses only in head cholinergic neurons), and *acr-2* (ventral cord cholinergic motor neurons). Expression driven by the *rab-3, unc-17,* and *unc-17H* promoters rescued the mutant locomotion defect, but expression driven by *acr-2* did not (***, P<0.001; ns, not significant, P>0.05). Error bars = SEM; n = 12-20.

(B) *eipr-1* acts cell autonomously to control dense-core vesicle cargo trafficking. The *eipr-1* cDNA was expressed in an *eipr-1* mutant background using either the *rab-3* promoter (all neurons) or *unc-129* promoter (a subset of cholinergic motor neurons where NLP-21::Venus is also expressed). Expression driven by both promoters rescued the *unc-129p*::NLP-21::Venus trafficking defect of the mutant (***, P<0.001). Left: representative images. Scale bar: 10 μm. Right: quantification of dorsal cord fluorescence. Error bars = SEM; n = 7-13.
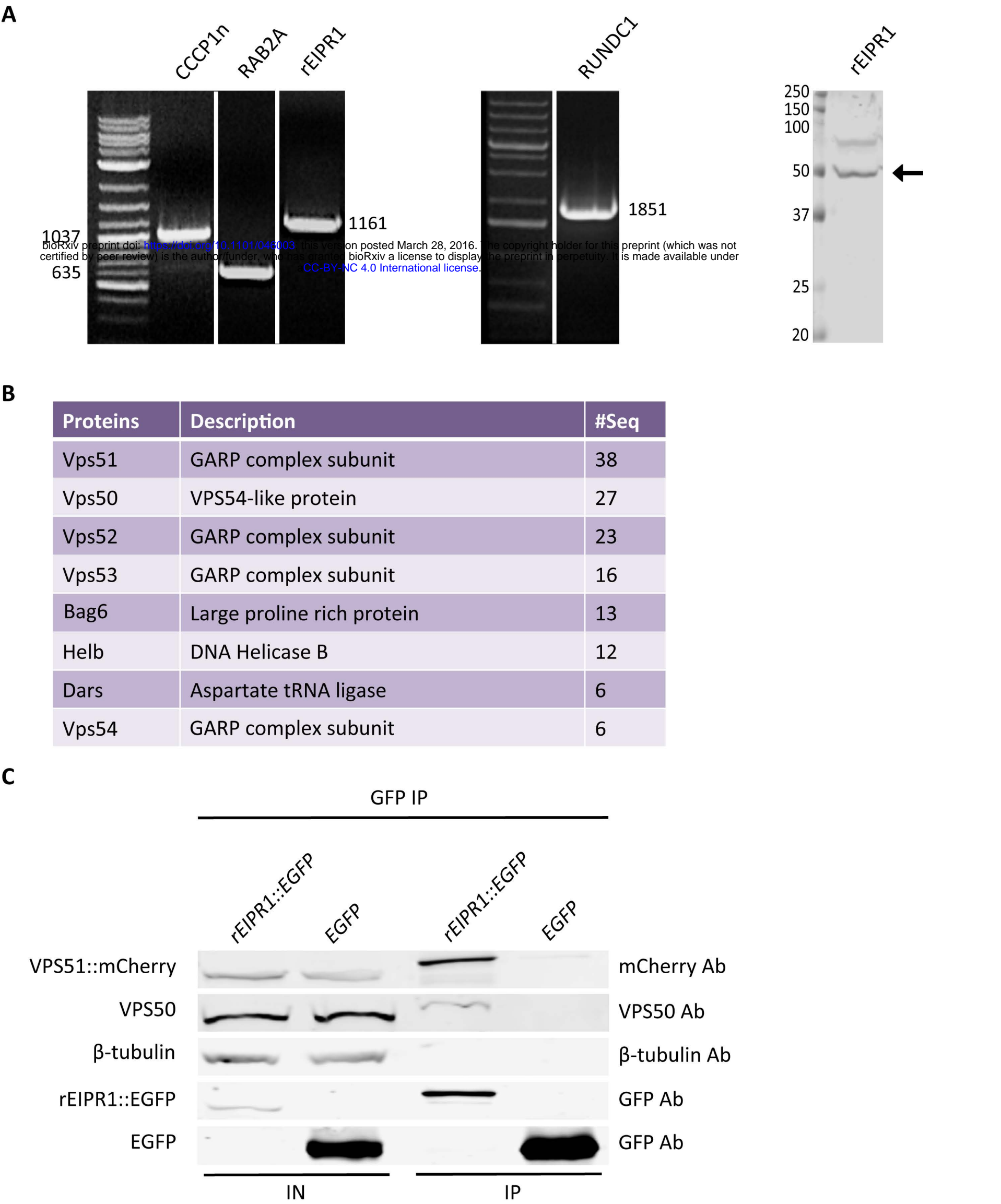
Figure 4

A

B

Proteins	Description	#Seq
Vps51	GARP complex subunit	38
Vps50	VPS54-like protein	27
Vps52	GARP complex subunit	23
Vps53	GARP complex subunit	16
Bag6	Large proline rich protein	13
Helb	DNA Helicase B	12
Dars	Aspartate tRNA ligase	6
Vps54	GARP complex subunit	6

C

Figure 4. EIPR-1 interacts with members of the GARP and EARP complexes.

(A) The rat ortholog of EIPR-1 is expressed in 832/13 cells. Left and middle: RT-PCR shows that rat orthologs of CCCP-1, RAB-2, EIPR-1 and RUND-1 are expressed in 832/13 cells. All bands are of the predicted size for the full-length cDNA except for CCCP1, which is truncated and corresponds to the N-terminal half of the gene. Right: Western blot shows expression of the rat EIPR-1 ortholog in 832/13 cells (arrow) at approximately its expected size (43 kD).

(B) EIPR1 interacts with members of the GARP and EARP complexes. List of top hits from mass spectrometry of a pulldown of rEIPR1::GFP in 832/13 cells after subtracting hits found in GFP control pulldowns. # seq = number of unique peptides from each protein. All proteins with more than 5 unique peptides are shown from one of two independent experiments. More complete data tables for both experiments are shown in Figure S5.

(C) EIPR1 interacts with VPS51 and VPS50. EGFP-tagged rat EIPR1 or EGFP was coexpressed with mCherry-tagged rat VPS51 in 832/13 cells. Immunoprecipitation of EIPR1::EGFP pulled down VPS51::mCherry and endogenous VPS50. Immunoprecipitation of untagged EGFP did not pull down VPS51::mCherry or VPS50. IN: input; IP: immunoprecipitation.
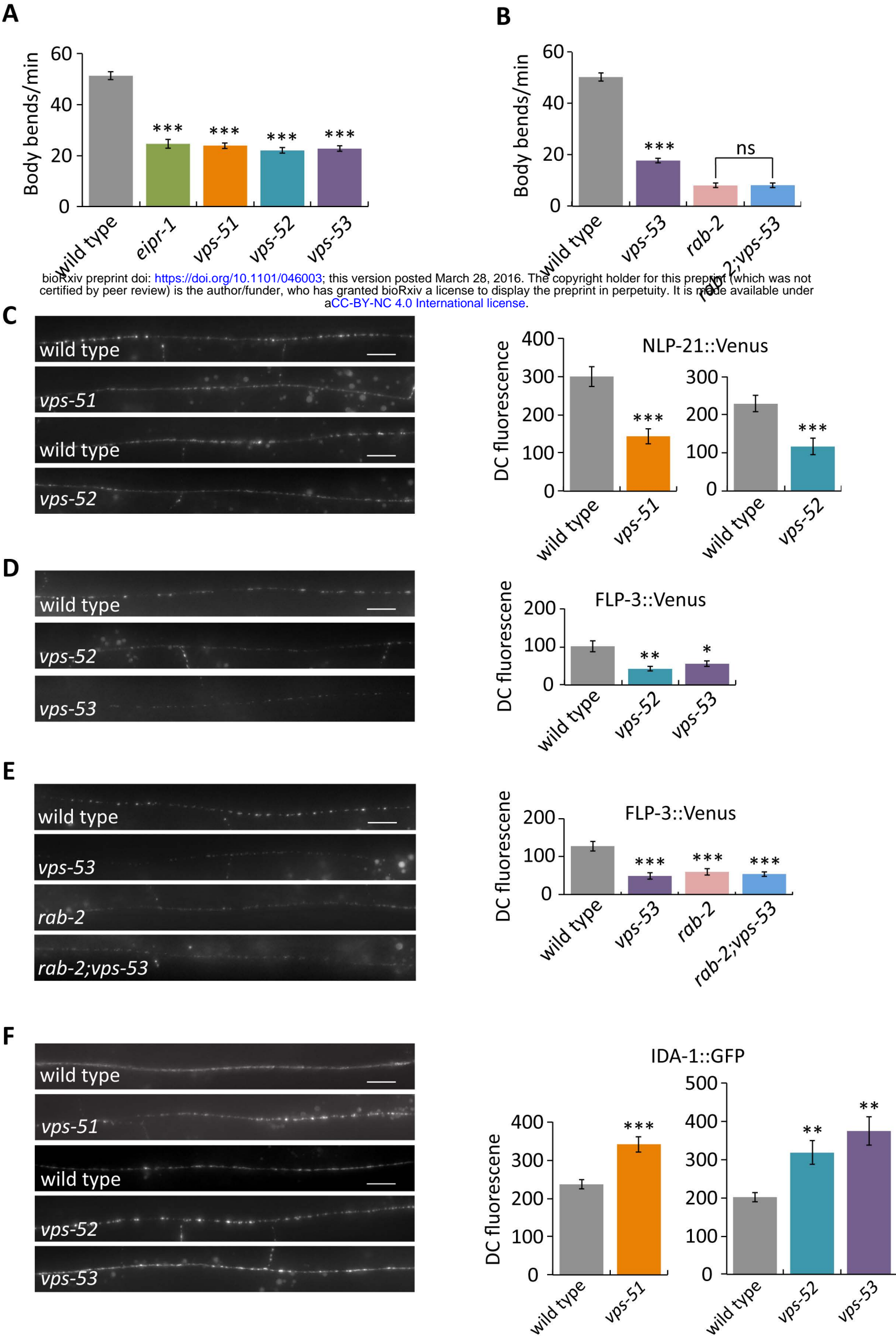
Figure 5

Figure 5. GARP/EARP mutants have defects in locomotion and trafficking dense-core vesicle cargos.

(A) GARP/EARP mutants *vps-51, vps-52,* and *vps-53* have a reduced locomotion rate. ***, P<0.001 compared to wild type. Error bars = SEM; n = 10.

(B) *vps-53* acts in the same genetic pathway as *rab-2* to control locomotion. A *rab-2; vps-53* double mutant does not have a stronger phenotype than a *rab-2* single mutant. ***, P<0.001 compared to wild type; ns, not significant, P>0.05. Error bars = SEM; n = 10.

(C) *vps-51* and *vps-52* mutants have reduced levels of NLP-21::Venus fluorescence in the dorsal nerve cord. Left: representative images. Scale bar: 10 µm. Right: quantification. The mean dorsal cord (DC) fluorescence intensity is given in arbitrary units. *vps-51* and *vps-52* were assayed in separate experiments with independent matched wild type controls. ***, P<0.001 compared to wild type. Error bars = SEM; n = 9-10.

(D) *vps-52* and *vps-53* mutants have reduced levels of FLP-3::Venus fluorescence in the dorsal nerve cord. Scale bar: 10 µm. ***, P<0.001; **, P<0.01 compared to wild type. Error bars = SEM; n = 10.

(E) *vps-53* acts in the same genetic pathway as *rab-2* to control FLP-3::Venus trafficking. A *rab-2; vps-53* double mutant does not have a stronger phenotype than *rab-2* or *vps-53* single mutants. Scale bar: 10 µm. ***, P<0.001 compared to wild type. Error bars = SEM; n = 10.
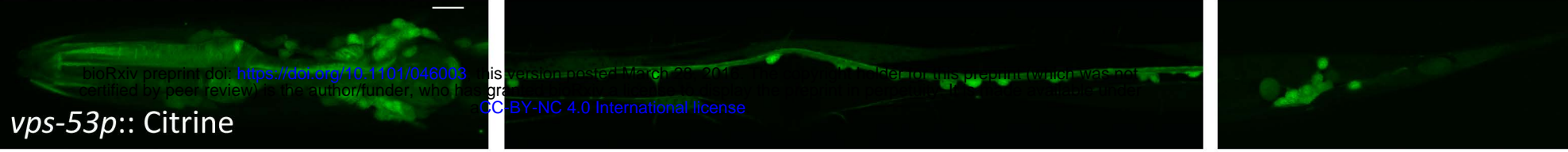
(F) *vps-51, vps-52* and *vps-53* mutants have increased levels of IDA-1::GFP in the dorsal cord. *vps-51* was assayed in a separate experiment from *vps-52* and *vps-53*, each with independent matched wild type controls. Scale bar: 10 µm. ***, P<0.001; *, P<0.05 compared to wild type. Error bars = SEM; n = 10.

Figure 6

A

vps-52p:: Citrine

B

vps-53p:: Citrine

C

GFP::RAB-2   VPS-52::RFP   merge

D

GFP::RAB-2   VPS-53::RFP   merge
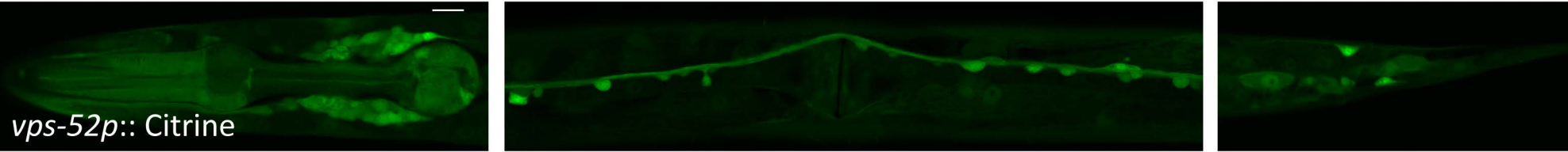
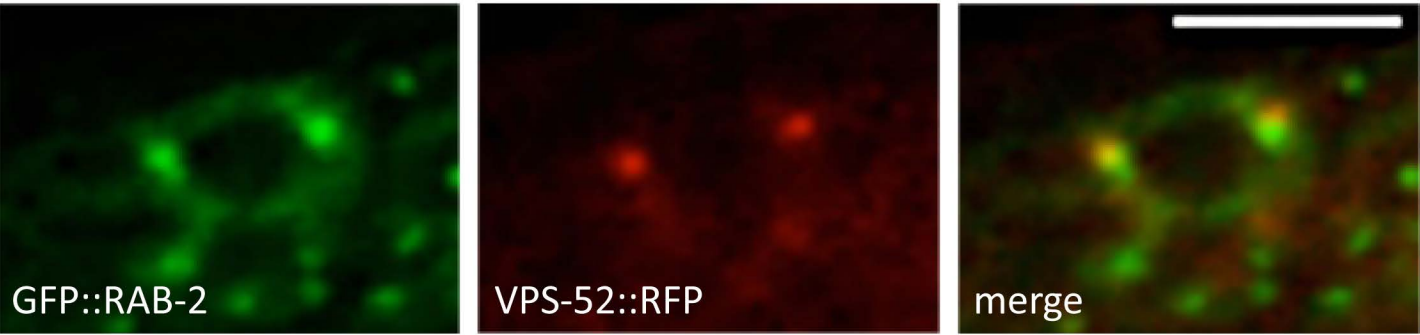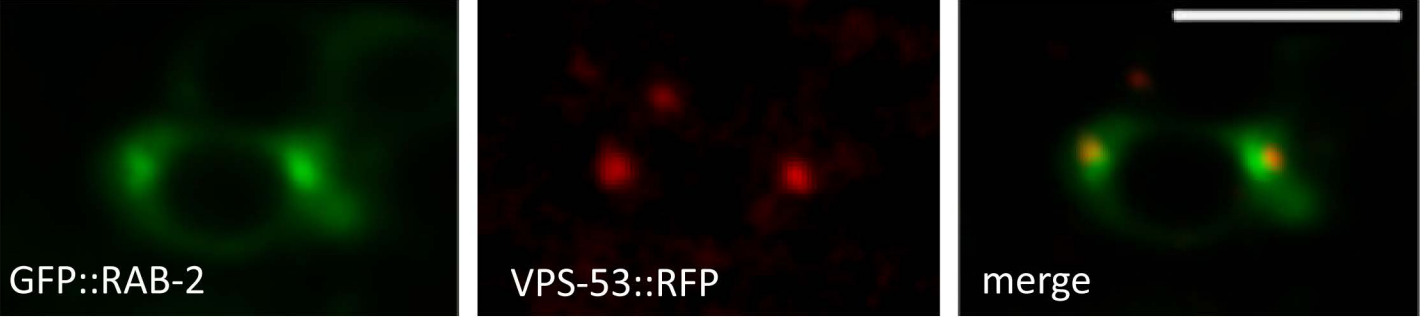**Figure 6. VPS-52 and VPS-53 are expressed in neurons and partially colocalize with RAB-2.**

(A) Representative images of animals expressing GFP under the *vps-52* promoter. The image on the left shows expression in the head neurons and pharynx, the image in the middle shows expression in ventral cord motor neurons and the image on the right shows expression in tail neurons. All images are single confocal slices of animals in a dorsal/ventral orientation. Scale bar: 10 µm.

(B) Representative images of animals expressing GFP under the *vps-53* promoter. The image on the left shows expression in the head neurons and pharynx, the image in the middle shows expression in ventral cord motor neurons and the image on the right shows expression in tail neurons. All images are single confocal slices of animals in a dorsal/ventral orientation except the tail, which shows a lateral orientation. Scale bar: 10 µm.

(C) Representative images of neurons coexpressing VPS-52::tagRFP and GFP::RAB-2. Scale bar: 5 µm.

(D) Representative images of neurons coexpressing VPS-53::tagRFP and GFP::RAB-2. Scale bar: 5 µm.
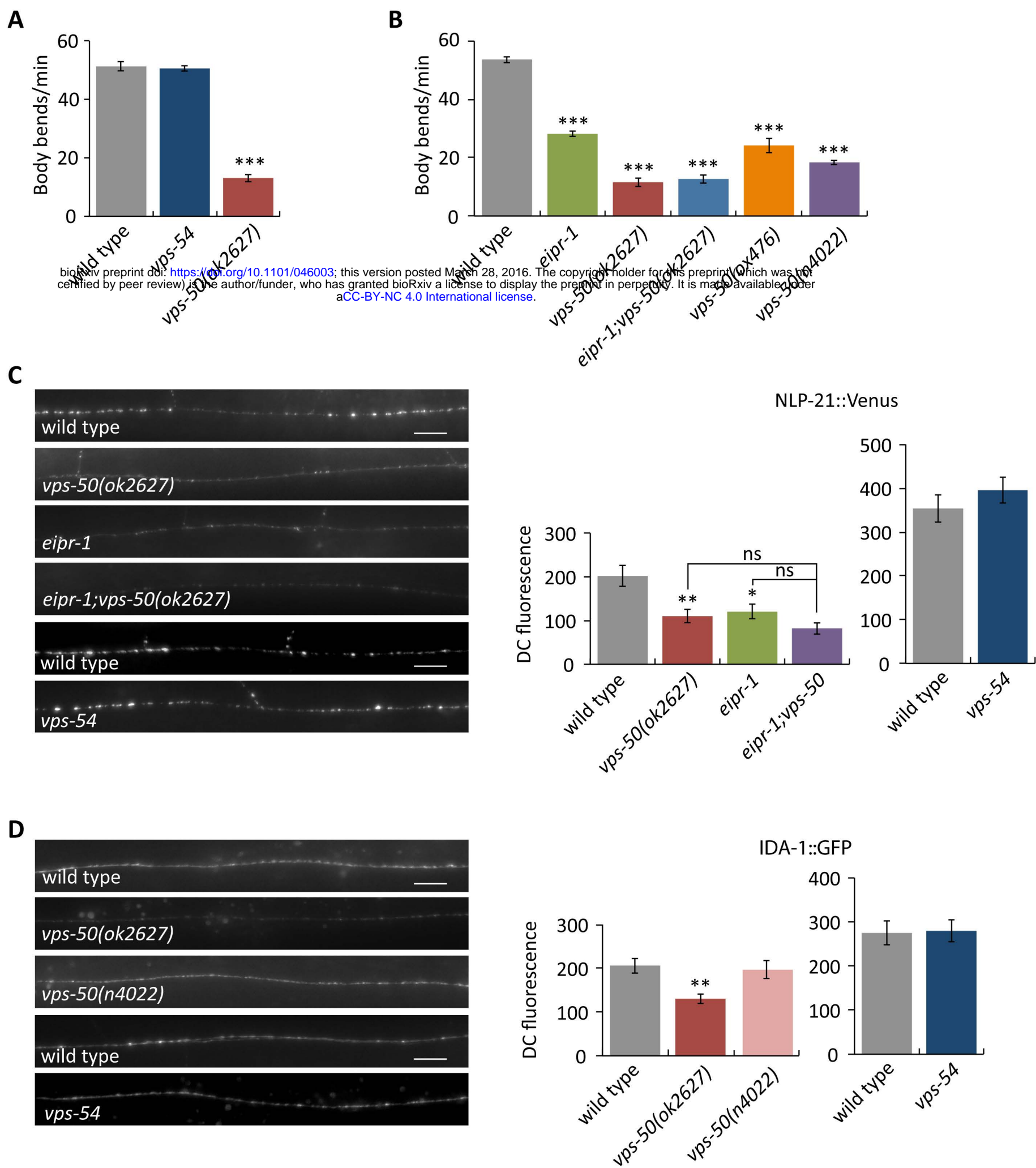
Figure 7

Figure 7. EARP, not GARP, is important for locomotion and trafficking dense-core vesicle cargos.

(A) The EARP-specific mutant *vps-50* has a reduced locomotion rate, but the GARP-specific mutant *vps-54* does not have reduced locomotion. ***, P<0.001 compared to wild type. Error bars = SEM; n = 10.

(B) *eipr-1* acts in the same genetic pathway as *vps-50* to control locomotion. An *eipr-1; vps-50* double mutant does not have a stronger phenotype than a *vps-50* single mutant. ***, P<0.001 compared to wild type. Error bars = SEM; n = 10.

(C) The EARP-specific mutant *vps-50* has reduced levels of NLP-21::Venus fluorescence in the dorsal nerve cord, but the GARP-specific mutant *vps-54* does not. Left: representative images. Scale bar: 10 μm. Right: quantification. The mean dorsal cord (DC) fluorescence intensity is given in arbitrary units. *vps-50* and *eipr-1* have reduced NLP-21::Venus fluorescence, but an *eipr-1; vps-50* double mutant does not have a stronger phenotype than either single mutant (ns, not siginificant, P>0.05), indicating that *eipr-1* and *vps-50* act in the same genetic pathway. A *vps-54* mutant had no reduction in NLP-21::fluorescence. *vps-54* was assayed in a separate experiment with independent matched wild type control. **, P<0.01; *, P<0.05 compared to wild type. Error bars = SEM; n = 10-11.

(D) IDA-1::GFP fluorescence levels in the dorsal cord. The *vps-50(ok2627)* deletion mutant had decreased IDA-1::GFP fluorescence (**, P<0.01) but the *vps-50(n4022)* late stop mutant and a *vps-54* deletion mutant had no decrease. *vps-54* was assayed in a separate experiment with independent matched wild type control. Scale bar: 10 μm. Error bars = SEM; n =10-12.
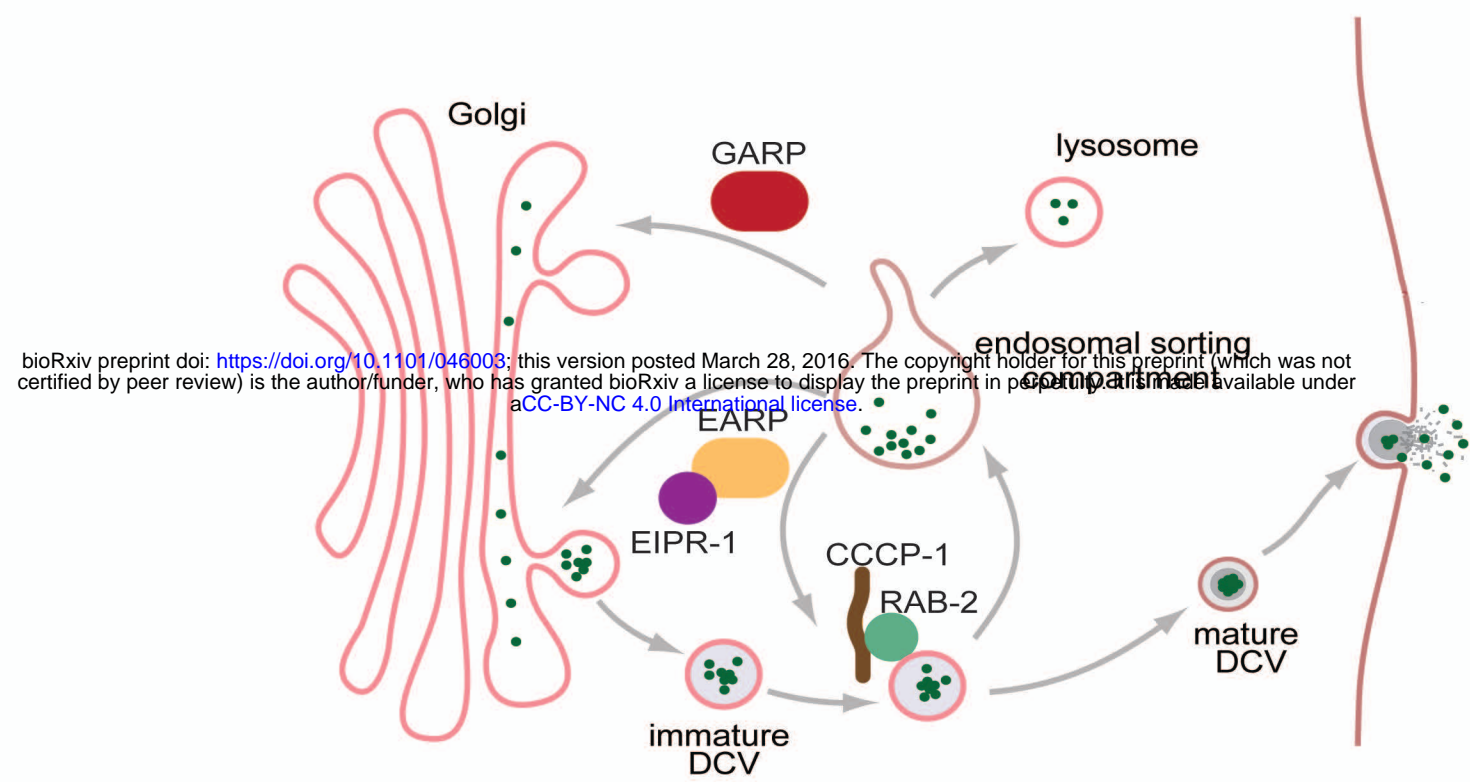
Figure 8

Figure 8. Model for dense-core vesicle cargo sorting by the EARP complex.

This model combines and builds on aspects of the well-described 'sorting by entry' and 'sorting by retention' models for sorting cargos to dense-core vesicles (15,16). Aggregation of cargo (clustered green dots) within the trans-Golgi may initiate the process of cargo sorting ('sorting by entry'). Then, following vesicle budding, non-aggregated cargo may be sorted away to endosomes while the aggregated core remains in the vesicle ('sorting by retention'). Additional aggregation may occur in post-Golgi immature vesicles as the pH drops and propeptides are processed. Finally, EIPR-1/EARP and RAB-2 and its effectors (e.g. CCCP-1, shown) may mediate the retrieval of non-aggregated cargos from the endosomal compartment back to the trans-Golgi or immature DCVs. Such a cyclical sorting mechanism may serve both to remove non-DCV cargos and to provide non-aggregated DCV cargos a "second chance" at sorting to DCVs by recycling them for a new round of potential aggregation. Multiple rounds of such a cycle could lead to enriched retention of aggregated cargos in DCVs. In mutants of EARP or RAB-2, reduced retrieval of cargos from endosomes may lead to their ultimate loss to lysosomes and hence reduced cargo levels in mature DCVs. GARP acts in a distinct endosome to Golgi trafficking pathway. It is also possible that EARP and RAB-2 act by retrieving unidentified sorting receptors.